Interactions between trade-wind clouds and local forcings over the Great Barrier Reef: A case study using convection-permitting simulations

Wenhui Zhao[1], Yi Huang[1,2], Steven Siems[2,3], Michael Manton[3], Daniel Harrison[4]

[1] School of Geography, Earth and Atmospheric Science, The University of Melbourne, Melbourne, VIC, Australia
[2] Australian Research Council (ARC) Centre of Excellence for Climate Extreme (CLEX), Melbourne, VIC, Australia
[3] School of Earth, Atmosphere and Environment, Monash University, Melbourne, VIC, Australia
[4] National Marine Science Centre, Southern Cross University, Coffs Harbour, NSW, Australia

Correspondence to: Wenhui Zhao (wenhui.zhao@unimelb.edu.au)

Abstract. Trade-wind clouds are ubiquitous across the subtropical oceans, including the Great Barrier Reef (GBR), playing an important role in modulating the regional energy budget. These shallow clouds, however, are by their nature sensitive to perturbations in both their thermodynamic environment and microphysical background. In this study, we employ the Weather Research and Forecasting (WRF) model with a convection-permitting configuration at 1 km resolution to examine the sensitivity of the trade-wind clouds to different local forcings over the GBR. A range of local forcings including coastal topography, sea surface temperature (SST), and local aerosol loading is examined.

This study shows a strong response of cloud fraction and accumulated precipitation to orographic forcing both over the mountains and upwind over the GBR. Orographic lifting, low-level convergence and lower troposphere stability are found to be crucial in explaining the cloud and precipitation features over the coastal mountains downwind of the GBR. However, clouds over the upwind ocean are more strongly constrained by the trade wind inversion, whose properties are, in part, regulated by the coastal topography. On the scales considered in this study, the warm cloud fraction and the ensuant precipitation over the GBR show only a small response to the local SST forcing, with this response being tied to the surface flux and lower troposphere stability. Cloud microphysical properties, including cloud droplet number concentration, liquid water path, and precipitation are sensitive to the changes in atmospheric aerosol population over the GBR. While cloud fraction shows little responses, a slight deepening of the simulated clouds is evident over the upwind region in correspondence to the increased aerosol number concentration. A downwind effect of aerosol loading on simulated cloud and precipitation properties is further noted.

1 Introduction

Trade wind cumuli are ubiquitous across the subtropical oceans (Warren et al., 1988; Norris, 1998; Eastman et al., 2011; Boucher et al., 2013; Rauber et al., 2007), including the Great Barrier Reef (GBR) (Zhao et al., 2022). Despite their limited vertical and horizontal extent, these clouds play a fundamental role in maintaining the thermodynamic budget of the lower troposphere (Chen et al., 2000). These clouds reflect a significant fraction of incoming solar radiation and emit long-wave radiation at relatively high temperature, and thus exert a net cooling effect on the earth atmosphere system (Mumby et al., 2001; Jones et al., 2017). Globally, these clouds help govern earth's energy budget, but are known to be a leading source of uncertainty in future climate projections (Boucher et al., 2013).

The GBR has become increasingly threatened by thermal coral bleaching events (CBEs) over the past decade (Hughes et al., 2017; Stuart-Smith et al., 2018). Recent research has also found that local-scale cloud cover helps regulate the ocean temperature along the GBR with anomalies in the cloud fraction having been directly linked to thermal CBEs (Zhao et al., 2021; Leahy et al., 2013). However, while the large-scale circulation has a fundamental influence on shallow cloud formation, these cloud systems by their nature are sensitive to perturbations in both their thermodynamic environment and microphysical background (Stevens and Brenguier, 2009; Rauber et al., 2007). It is, therefore, important to understand the sensitivity of these low clouds in response to different local forcings.

The GBR contains the world's largest complex collection of coral reefs. It has been hypothesised that the coral reef emissions of dimethyl sulfide (DMS) may be an important contributor to the regional atmospheric aerosol loading (Cropp et al., 2018). Any perturbation to the aerosol population could potentially affect the cloud properties and thus the radiative forcing (Lohmann and Feichter, 2005), for instance through a Twomey effect (Twomey, 1997). It has further been hypothesized that the aerosol loading can also affect the precipitation efficiency of these clouds, and thus their lifetime (Cropp et al., 2018; Fischer and Jones, 2012; Deschaseaux et al., 2016; Jones, 2015) through an Albrecht effect (Albrecht, 1989).

Over the GBR, a recent climatology study by Zhao et al. (2022) revealed little to no difference in low-level cloud properties between the open ocean (reef-free region) and the coral reef region, using long-term satellite datasets. These results suggest that low clouds over the GBR do not show a measurable response to the reef-related microphysical perturbations, at least using spaceborne observations. However, subtle signals may be obscured or diminished when averaged over extensive periods in long-term climatological analyses. While a very small natural contribution to the cloud condensation nuclei (CCN) population from coral derived DMS was noted over the GBR by either global (Fiddes et al., 2021) or regional scale (Fiddes et al., 2022; Jackson et al., 2022) simulation studies, broader impacts of aerosol on cloud and precipitation processes over the GBR remain unquantified. For example, anthropogenic emissions are found to be important over the GBR in regard to modulating the influence from coral-reef-derived aerosol on local aerosol burdens. In addition, a higher temporal resolution analysis including the diurnal cycle of these low-level clouds may be critical in understanding their effect on the radiation budget (Fiddes et al., 2022, Fiddes, 2020). It is, therefore, appropriate to employ high-resolution convection-permitting modelling as an investigation tool to elucidate the full life cycle of these clouds, the development of the precipitation and their response to any perturbations in the aerosol loading (Colle et al., 2005; Smith et al., 2015).

Variations in Sea Surface Temperature (SST), from the shallow water area off the coast to the deeper open ocean and from low to high latitudes over the GBR, could also lead to differences in cloud properties, especially for boundary layer clouds (Crook 1996). SST directly contributes to the thermodynamic conditions, which modulate the sensible and latent heat fluxes, and, consequently, cloud properties such as cloud cover, cloud top height and cloud base (Bony et al., 2004). Significant positive SST anomalies are known to be a key driver of severe thermal coral bleaching periods across the GBR (Berkelmans et al., 2004; Hughes et al., 2017). These large SST anomalies, which could be prevalent for a few months and may spike during periods of weak winds (Filipiak et al., 2012; Gentemann et al., 2003; Zhang et al., 2016), are hence expected to produce a strong local forcing that could change the local thermodynamic conditions.

In addition to the aerosol and SST variations, clouds over the GBR can experience other local forcing mechanisms unique to this region. For example, orographic forcing could potentially be important when the south easterly trade winds blow clouds across the Queensland coast and encounter the Great Dividing Range (Houze, 2012). The Wet Tropics of Queensland stretches along the northeast coast of Australia for around 450 km roughly 15-19 °S (between the towns of Cairns and Townsville), where significant topography of ~1000m with a peak height of 1612 m at Mount Bartle Frere (Sumner and Bonell, 1986) is present. Pronounced precipitation enhancement over the windward slopes of the mountain barrier (Roe, 2005) is commonly observed. The mean annual accumulated rainfall over this large area is among the greatest in Australia (e.g. Bonell and Gilmour, 1980), with the Bellenden Ker Top station receiving over 8000 mm of annual precipitation (Herwitz, 1986) on average. Zhao et al. (2022) found significant orographic enhancement of low-level clouds not only over the Wet Tropics, but also over the upwind ocean extending partially over the GBR. It is therefore of interest to examine any upwind effect of orographic enhancement on shallow cloud and precipitation through high-resolution numerical simulations, where interactions of local variability associated with topography and coastal processes are better resolved.

In this paper, we undertake a case study using a series of simulations to explore the sensitivity of trade wind cumulus over the GBR to these different local forcings. In particular, we seek to address three scientific questions: (a) How does the topography of the Great Dividing Range affect the shallow clouds and precipitation over the Wet Tropics including the GBR? (b) Is there any evidence of changes in cloud and precipitation properties in response to SST variations across the GBR? (c) How do the shallow cloud and precipitation properties respond to enhanced local aerosol loading, both over the GBR and downwind over the coast of Queensland? Unlike the study of Fiddes et al. (2021) and Fiddes et al. (2022), this study does not aim to test the effects of DMS directly. Rather, it focuses on understanding how strongly, if at all, cloud and precipitation properties respond to changes in the atmospheric aerosol number concentration related to surface emissions. This analysis is also relevant to understanding the integrated effects of potential weather and climate interventions, such as marine cloud brightening, in the heat-sensitive environment of the GBR and its adjacent communities.

To address these questions, a range of sensitivity experiments is conducted using convection-permitting numerical simulations. This paper is divided into five sections as follows: Section 2 gives a brief description of the background climate and the meteorological conditions of the region, Section 3 details the data and methods used in this study. The main results and discussion are presented in Section 4 and Section 5. Section 6, finally, summarizes the results and provides prospects for future research.

2 29 April 2016 Case Study

The GBR is characterized by a warmer than average monthly sea surface temperature during April 2016 when a thermal coral bleaching event was reported (Zhao et al., 2021). An SST anomaly of over 1°C is identified across much of the GBR (Figure S1), with this SST anomaly being likely to affect the cloud properties, especially low-level clouds through marine atmospheric boundary layer (MABL) processes (Qu et al., 2015; Takahashi et al., 2021). This selected case is characterized by local trade wind cumulus over the Wet Tropics and associated with orographic precipitation on 29th April 2016. This event is also chosen due to the absence of high cloud cover across the Wet Tropics, which are often linked to deeper convection governed by large-scale climate modes such as El Niño-Southern Oscillation (ENSO) and Madden-Julian Oscillation (MJO), as well as the Australian monsoon or tropical cyclones (Tian et al., 2006; Yuan et al., 2013; Eleftheratos et al., 2011; Wu et al., 2012). Note that there is a weak El Niño phase of ENSO during the case study period. Further, the MJO is weak, with the Real-time Multivariate MJO index (Wheeler and Hendon, 2004) less than 1, and no tropical cyclones are recorded across the Northeast Queensland and the GBR.

The mean sea level pressure (MSLP) analysis at 1200 UTC of 28th and 29th April 2016 (Figure 1a-b) reveals a Tasman High maintaining the south-easterly trade winds along the northeast coast of Queensland during the case period. Originating in southwest Australia on 22 April, this high-pressure system gradually progressed eastward (not shown). By 26 April, it was positioned over southeast Australia, consequentially producing a high ridge along the northeast coast of Queensland during the following four days. As shown in the Himawari-8 true color images (Figure 1c) at 0000 UTC 28th April 2016, northeast Queensland has mostly a clear sky with patches of low-level clouds (stratocumulus, cumulus and stratus, as shown in Figure 1e) extending southwest from the coast in the Wet Tropics. Satellite observations at 0500 UTC 29th April 2016 (Figure 1f) reveal a well-developed cloud system consisting of stratocumulus, altocumulus and altostratus. Orographic precipitation associated with trade wind cumuli is captured by land-based rain gauges at several weather stations (Figure 2) on 29th April. The heaviest precipitation was recorded over the eastern slopes and mountain peaks, which is expected under the influence of upslope lifting under the prevailing southeasterly wind regime. From 0600 UTC 30th April, the cloud system over the Wet Tropics started dissipating, as observed by satellite images (not shown).

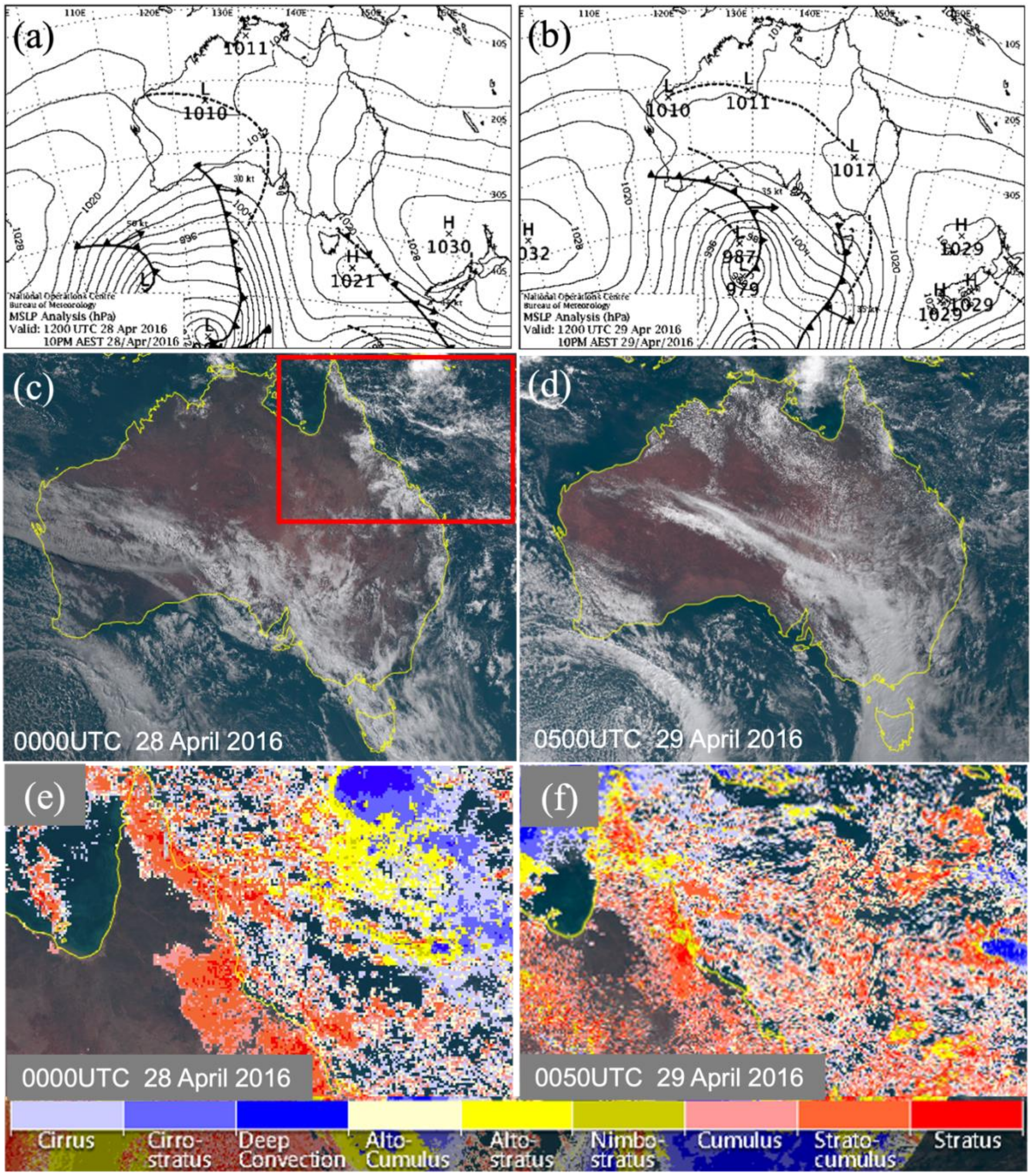

Figure 1: Mean Sea-Level Pressure (MSLP) analyses for 2016 April case at (a) 1200UTC 28th and (b) 1200UTC 29th. Himawari-8 true color imagery for (c) 0000UTC on 28th April and (d) 0500UTC on 29th April 2016. Himawari-8 cloud type classification for (e) 0000UTC on 28th April and (f) 0500UTC on 29th April 2016 for the domain shown by red rectangle in (c). Cloud types as listed on the colorbar for (e-f) are Cirrus, Cirrostratus, Deep Convection, Altocumulus, Altostratus, Nimbostratus, Cumulus, Stratocumulus, and Stratus. Images (a-b) are provided by the Australian Bureau of Meteorology. Images (c-f) are supplied by the P-Tree System, Japan Aerospace Exploration Agency (JAXA).

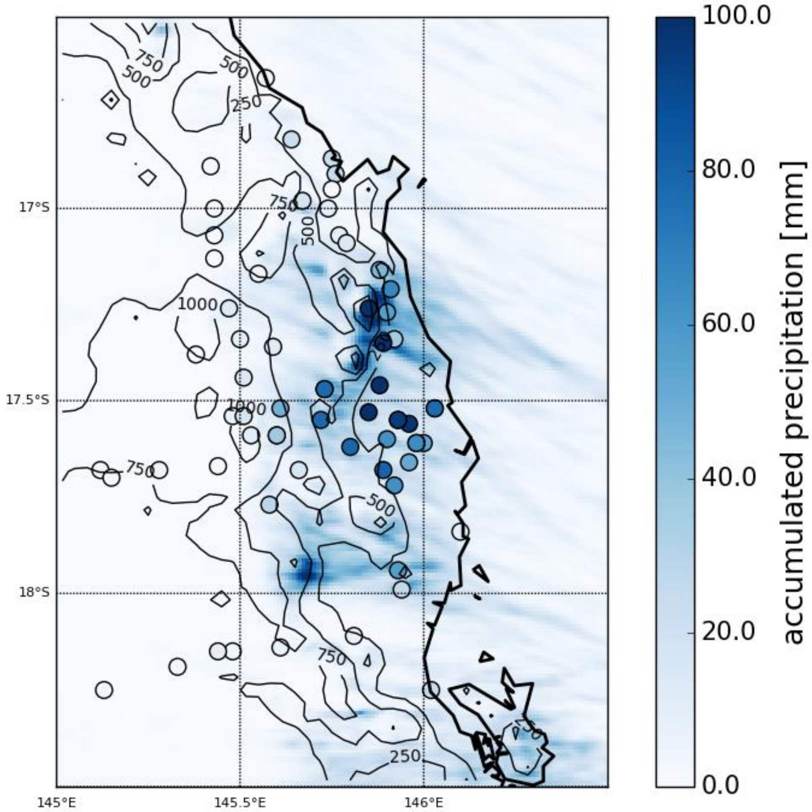

Figure 2: The 48-h accumulated simulated precipitation amounts from 1km resolution with CTRL from 2016-04-27 23:00UTC to 2016-04-29 23:00 UTC overlaid with the precipitation observed by rain gauges shown as filled circles using the same color scale. Black contours indicate the topography map from 250 to 1500 m by 250 m-interval.

3 Data and Methodology

3.1 Model configuration

The Weather Research and Forecasting (WRF, version 4.2; Skamarock et al., 2019) model is used to simulate the interactions between trade wind cumulus and local forcings. In this study, the model is configured with unevenly distributed 65 levels in the vertical (Figure S2), allowing for 30 levels in the lowest 3 km where most of the trade cumulus clouds reside. Three nested domains with horizontal grid spacing of 9 km, 3 km, and 1 km are utilized (Figure 3a). The innermost domain (d03) is set up with 562 × 457 grid points covering most of the significant topography over the Wet Tropics (Figure 3b), extending over the GBR. The model uses the fifth-generation atmospheric reanalysis (hourly, 0.25° × 0.25° grid, 37 set pressure levels and surface level) from the European Centre for Medium Range Weather Forecast (ERA5 reanalysis, Hersbach et al., 2018; 2020), for initial and lateral boundary conditions, as part of the standard WRF pre-processing system (WPS). Following initialization, the model is allowed to run freely with no nudging applied, which enables the meteorology to fully develop throughout the simulation. The control (CTRL) simulation is initialized at 1200 UTC 27 April 2016 and run for three days (i.e. 72 hours) with the first 12 hours being used as the spin-up time. It is worth noting that sensitivity to different spin-up times (e.g. 12h, 18h, and 24h) has been tested as the optimal spin-up time configuration may vary across different case studies, reflecting the unique atmospheric conditions and dynamics inherent to each scenario. The results indicate that the simulation with a shorter spin-up time (12h) produces a better agreement with observations for this case (not shown).

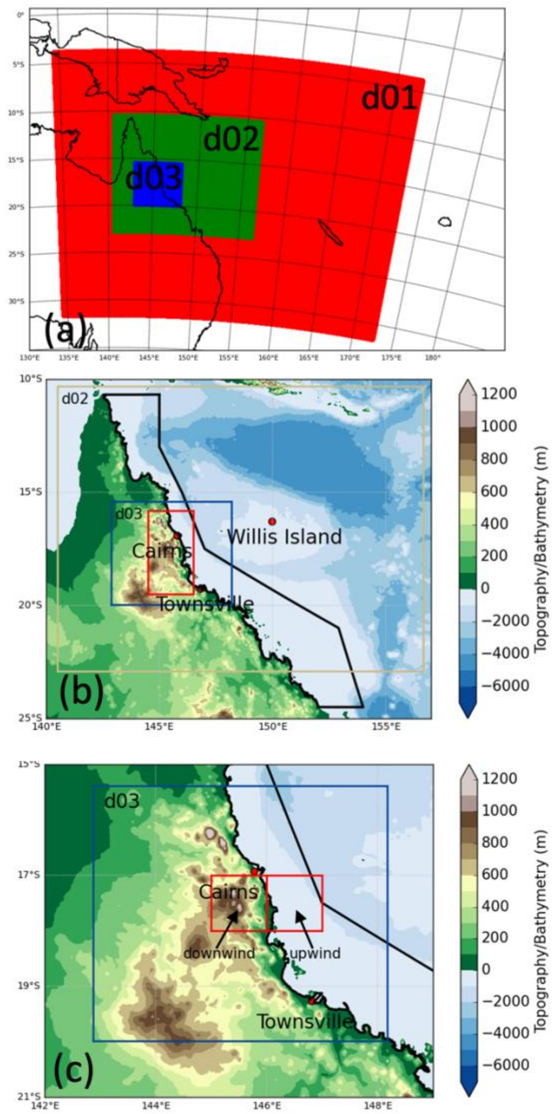

Figure 3: (a) The WRF three nested domains shown by different color boxes used in this study. (b) Zoomed-in topographic-bathymetric map of the two inner domains (shown by colored rectangles) with the locations of two sounding stations (Townsville and Wills Island). The solid red rectangle points out the location of the Wet Tropics. Black lines indicate the GBR general reference map. (c) 1° × 1° downwind and upwind sub-domains shown by red rectangles.

The history intervals of prediction outputs are set to be 6 hours for d01, 3 hours for d02, and 1 hour for d03. Simulations are performed with the Yonsei University (YSU, Hong et al., 2006, first-order nonlocal) planetary boundary layer (PBL) scheme, "Noah" land surface model (Chen and Dudhia, 2001), and the RRTMG (Mlawer et al., 1997) scheme for shortwave and longwave radiation, respectively. The same schemes are used for each domain, with the exception of the cumulus scheme. The Kain-Fritsch (Janjić 2000) cumulus parameterization is used only for the coarsest domain (d01) to represent sub-grid convection. For the microphysical parameterization, the Thompson Aerosol Aware microphysics scheme (Thompson and Eidhammer, 2014), a bulk scheme that treats five separate water species: cloud water, cloud ice, rain, snow, and a hybrid graupel-hail category, is used. This scheme utilizes double-moment prediction (mass and concentration) of cloud water, cloud ice, and rain mixed with single-moment prediction (mass only) of snow and graupel. Updated from the previous version (Thompson, 2008), this version of microphysics scheme incorporates the activation of aerosols as cloud condensation (CCN) and ice nuclei (IN), and therefore, explicitly predicts the number concentration of two aerosol variables. Rather than assuming all model horizontal grid points have the same vertical profiles of CCN and IN aerosols, this study uses an auxiliary aerosol climatology as the aerosol background condition placed into WRF model for every grid points, regardless of cloudiness. The aerosol input data are derived from multiyear (2001-2007) global model simulations (Calarco et al. 2010) in which particles and their precursors are emitted by natural and anthropogenic sources. Multiple species of aerosols, including sulfates, sea salts, organic carbon, dust, and black carbon, are explicitly modelled with multiple size bins by the Goddard Chemistry Aerosol Radiation and Transport model with 0.5° longitude by 1.25° latitude spacing. The microphysical scheme then transforms these data into simplified aerosol treatment by accumulating dust mass larger than 0.5 μm into the IN (ice-friendly) mode and combining all other species besides black carbon as an internally mixed CCN (water-friendly) mode. To get the final number concentrations from mass mixing ratio data, it is assumed that lognormal distributions are used, with characteristic diameters and geometric standard deviations taken from Chin et al. (2002). Samples of the climatological aerosol dataset can be found in Thompson and Eidhammer (2014, Fig 1). Note that black carbon is ignored for this version but might be incorporated into future versions (Thompson and Eidhammer, 2014). However, it is not expected that the absence of black carbon aerosol will have a significant effect for pristine maritime trade cumulus clouds. Rather than considering multiple aerosol categories, the Thompson Aerosol Aware microphysics scheme simply refers to the hygroscopic aerosol (a combination of sulfates, sea salts, and organic carbon) as a "water friendly" aerosol and the nonhygroscopic ice-nucleating aerosol (primarily considered to be dust) as "ice friendly". The activation of aerosols as CCN and IN is determined by a lookup table that employs the simulated temperature, vertical velocity, number of available aerosols, and hygroscopicity parameter applied in Köhler activation theory. The activation of aerosols as droplets is performed at cloud base as well as anywhere inside a cloud where the lookup table value is greater than the existing droplet number concentration (Thompson and Eidhammer, 2014). Note that the aerosols used by the microphysics scheme to activate water droplets and ice crystals do not scatter or absorb radiation directly. The aerosol's scattering–absorption–emission of direct radiation is only considered within the RRTMG radiation scheme by the typical background amounts of gases and aerosols in this study (Thompson and Eidhammer, 2014). The Thompson Aerosol Aware scheme has been shown in previous studies to have promising skill in representing both supercooled and warm liquid conditions of grid-scale clouds (Weston et al., 2022; Wilkinson et al., 2013).

An overview of the parameterization schemes used in the CTRL simulation is provided in Table 1. It is worth noting that other configurations with different microphysics, boundary layer, and cumulus schemes have also been tested, and the simulation with the configuration listed in Table 1 is found to be most skilful when evaluated against observations. This configuration is therefore used as CTRL run and the same configuration settings are applied to all sensitivity experiments.

Table 1: A list of configuration settings for numerical study

Parameterisation	Option No. (d01, d02, d03)	Comments
Microphysics	mp_physics = 28	Thompson Aerosol Aware (2014) scheme
PBL	bl_pbl_physics = 1	YSU PBL scheme
Cumulus	cu_physics = 1 (d01 only)	Kain-Fritsch scheme (d01 only)
Land/Sea surface	sf_surface_physics = 2	Noah Land Surface Model
Short wave radiation	ra_sw_physics = 4	RRTMG shortwave
Long wave radiation	ra_lw_physics = 4	RRTMG scheme

3.2 Sensitivity experiments

Five sensitivity experiments are undertaken to examine the impacts of various local forcings, as detailed below:

In the topography experiment, the orography above 300 m is reduced by 75% (Figure S3), named “Topo300”, as similarly done in Flesh and Reuter (2012) and Sarmadi et al. (2019). A threshold of 300 m is chosen because it is approximately the mean altitude of the Wet Tropics region, hence representing the background geography. A 75% reduction is used in order to preserve some of the topographic features, and to avoid drastic changes of topography that may induce dramatic changes in the larger-scale circulations. We note that a 500 m threshold is also tested and yielded similar results (not shown).

For the local SST forcing, two sensitivity simulations have been conducted in which the monthly mean climatological SST condition for April (namely “SST-climatology”, Figure S1) and spatially uniformed 1°C cooler than real SST condition (namely “SST-cooler”) are used to initialize the simulation. The monthly SST climatology applied in the control simulation is derived from ERA5 for the period of 1998-2018. This climatology integrates SST data from HadISST2 (before September 2007) and OSTIA (September 2007 onwards) datasets. It is important to note that, unlike the SST alteration in the SST-cooler experiment, part of the ocean area in the SST-climatology is warmer than the actual SST (Figure S1). Nevertheless, the sea surface temperature over the majority of the GBR is reduced in the SST-climatology experiment. The selection of a 1 ˚C perturbation is based on the findings presented in Zhao et al. (2021), where a typical 1 ˚C positive SST anomaly is noted during the coral bleaching season over the GBR. SST modifications are applied to the whole ocean area for all three domains. It should be noted that, as with CTRL, the SST conditions are fixed through the 3-day simulations.

Finally, the climatological surface water-friendly aerosol (WFA) emissions (kg^{-1} s^{-1}) over the GBR (see general reference map in Figure 3b) is increased by a factor of 2 and 5, respectively, to test the sensitivity of warm cloud and precipitation to the aerosol loading to emulate a scenario of enhanced aerosol population associated with coral reef emissions (named “Aerosol2” and “Aerosol5”, respectively, Figure S4).

Table 2 summarizes the details of these sensitivity experiments.

Table 2: Detailed information of numerical experiments conducted in this study.

		Modification description
CTRL-run		N/A
Sensitivity experiments	Topo300	Decreases elevation by 75% for elevations above 300m
	Aerosol2	Climatological surface WFA emissions increased by 200%, GBR only
	Aerosol5	Climatological surface WFA emissions increased by 500%, GBR only
	SST-cooler	SST reduced by 1°C, whole ocean domain
	SST-climatology	SST replaced by 21-yr (from 1998 to 2018) April climatology, whole ocean domain

3.3 Observational Data

Several observational datasets and reanalysis are used to evaluate the simulation across a range of spatial-temporal scales. In this study, sounding data at 0000 UTC and 1200 UTC during the simulation period are obtained from the University of Wyoming upper-air sounding database for two selected radiosonde stations (Townsville, code: 94294, and Willis Island, code: 94299). To evaluate the large-scale meteorological background conditions in the simulation, hourly mean sea level pressure (MSLP) and wind field at 10 m are also obtained from ERA5 reanalysis with a resolution of 0.25° for the case period (Hersbach et al., 2020). Channel 13 brightness temperatures from the Himawari-8 satellite dataset (Bureau of Meteorology, 2021) and daily rainfall datasets from continuous weather stations are obtained from the Australian Bureau of Meteorology for the case study period. A total of 60 stations are selected, and their spatial distribution is shown in Figure 6. It should be noted that some of thermodynamic observations (e.g. radiosonde soundings and wind observations) are being assimilated into the reanalysis, however, observations of cloud and precipitation are not. It is expected that the initial hours will exhibit strong agreement of thermodynamic variables with the ERA5 dataset, but over the course of the 36 hours, the simulations will be sensitive to the parameterisations and settings selected. Therefore, the evaluation of model output is designed to examine the middle and last few hours of the simulation (Figures 4 and 5) against both ERA5 thermodynamics and independent cloud and precipitation observations (e.g. Himawari and weather station, Figures 2 and 6).

3.4 Identifying the trade wind inversion

The trade wind inversion (TWI), which results from the interaction of large-scale subsiding air from the upper troposphere and rising air from lower levels that is driven by convection, plays an important role in defining cloud structure and vertical development (Riehl et al., 1979; Albrecht, 1984). Under a trade-wind regime, the top of a cloud layer typically marks the base of the inversion.

In this study, we use the same criteria identified in Murphy et al. (2017) to examine the TWI characteristics and its interaction with clouds. Four variables are used: (1) pressure, (2) height, (3) dry bulb temperature, and (4) relative humidity. The criteria used are as follows:

a) The TWI is restricted to the 850-600 hPa layer and environmental temperatures greater than 273 K.
b) The base of the TWI is defined where the temperature begins to increase, and relative humidity decreases with height.
c) The top of the TWI is defined by a vertical temperature decrease with height.
d) When multiple inversions are detected, the layer with the greatest relative humidity decrease is selected as the TWI.

Two properties, in addition to the inversion base height, describing the TWI are defined also following the method described in Murphy et al. (2017). The inversion thickness (km) is the difference in height between the base and top of the inversion, while the inversion strength or magnitude (K) is the temperature increase across the inversion. It should be noted that grid points with no TWI identified (around 19% of total samples) are excluded from the TWI analysis.

4 Control simulation

In this section, the simulated synoptic and the surface features are first evaluated by comparing the results of the control simulation with observations. It is found that the control simulation skillfully simulated the evolution of the large-scale synoptic patterns of the MSLP in terms of both the progression and the magnitude of the surface pressure system (not shown). Simulated wind conditions at 850 hPa at 0000 UTC 28 April (the first hour after spin-up time) are compared with ERA5 reanalysis, and the 3 km WRF simulated pattern and magnitude of the wind field are found to be generally in good agreement with the reanalysis (Figures 4a and 4b). It should be noted that this is largely expected as the simulations are initialized with ERA5 reanalysis in this study. However, a good agreement is also found towards the end of the simulation (1200 UTC 30 April), suggesting that the simulation in this study is doing a good job regarding representation of the synoptic condition. As shown in Figures 4c and 4d, both wind speed and direction agree reasonably well with the reanalysis, though a disagreement in the wind speed is noted in the southern part of the ocean. Figure 5 shows the observed soundings (black) from the two available sounding stations (Willis Island and Townsville) within the domain and the simulated atmospheric profile (red) at the nearest grid point in the 3 km domain at 0000 UTC on 28 and 30 April. The simulated soundings at the two sites both have good agreement with observations at the beginning and the last day of the simulation, with both wind speed and direction well captured throughout the profile. The simulation accurately predicts the cloud base height (around 850 m) and surface temperature at the two sites, and it is worth noting that the wind inversion at 800 hPa at Townsville station is well captured throughout the simulation (Figure 5).

Figure 5 compares the observed and simulated brightness temperature throughout the simulation period. Note that the simulated brightness temperature is simply calculated assuming an emissivity of one for all surfaces and an effective cloud optical depth of one. It is used for a qualitative evaluation of the simulated cloud field only. Overall, the cloud field is reasonably well simulated in terms of the location and timing when compared against the Himawari-8 observation. Although the chaotic nature of shallow cumulus cloud means that details are not fully aligned, the major cumulus cloud features over the Wet Tropics throughout the three-day simulation period have been well captured.

Figure 2 shows the 48 h accumulated precipitation from the 1 km WRF simulation, overlaid with the observed rainfall shown as filled circles using the same color scale. The orographic signature (see Figure 3b and black contours in Figure 6), as shown in the correlation between the accumulated precipitation amounts and topography, is evident in both the observed and simulated precipitation. The overall distribution of the simulated accumulated precipitation shows a good agreement with the rain gauge observations, with the majority of the precipitation produced over the windward side of the topography. Although a bias is noted in the location of the peak precipitation, with the simulated precipitation indicating a northward shift relative to the observation, the simulated accumulated precipitation amounts agree reasonably well with the rain gauge observations. This shows the model has acceptable skill in predicting precipitation patterns and magnitude, despite some spatial discrepancies.

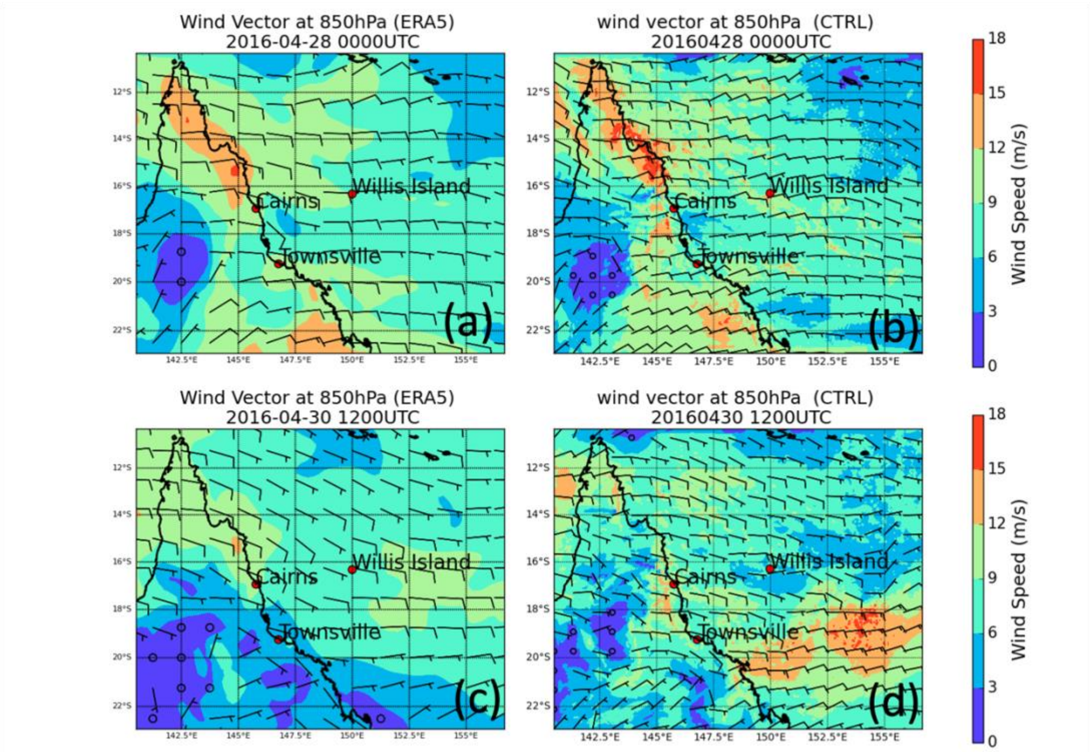

Figure 4: (a) Wind vector distribution at 850 hPa from ERA5 and (b) WRF simulations from CTRL-run at 0000UTC 28th April 2016. (c-d) same as (a-b), but for 1200UTC 30th April 2016. Note that same color scales are applied in all panels.

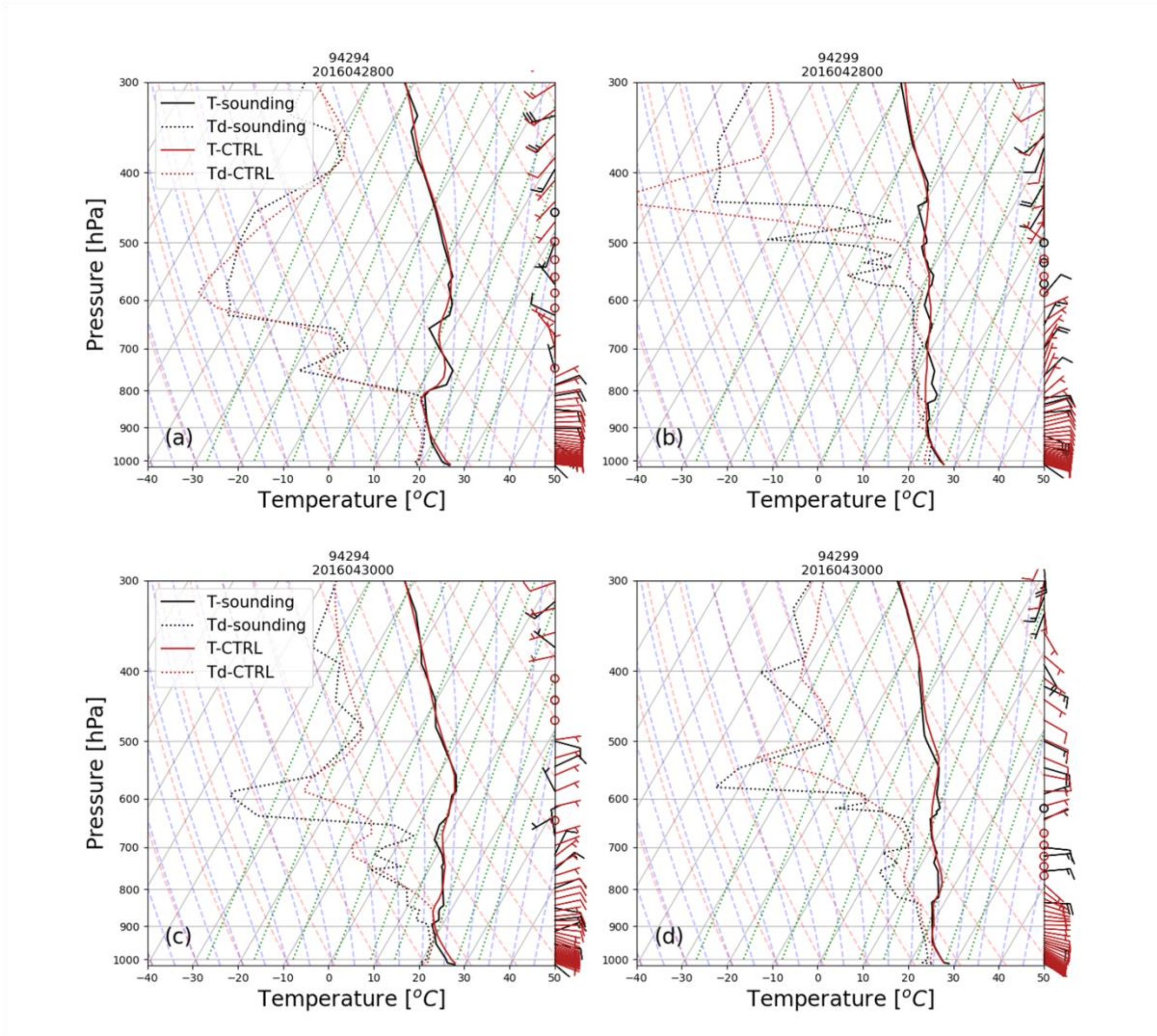

Figure 5: Comparison of the observed upper air soundings (black lines) from (a) Townsville and (b) Willis Island alongside 3 km WRF simulations (red lines) from the nearest grid point to two stations on 28 of April 2016 at 0000 UTC. (c-d) same as (a-b), but for the time of 0000UTC on 30 April 2016. Solid lines are for temperatures and dotted lines represent dew point temperature.

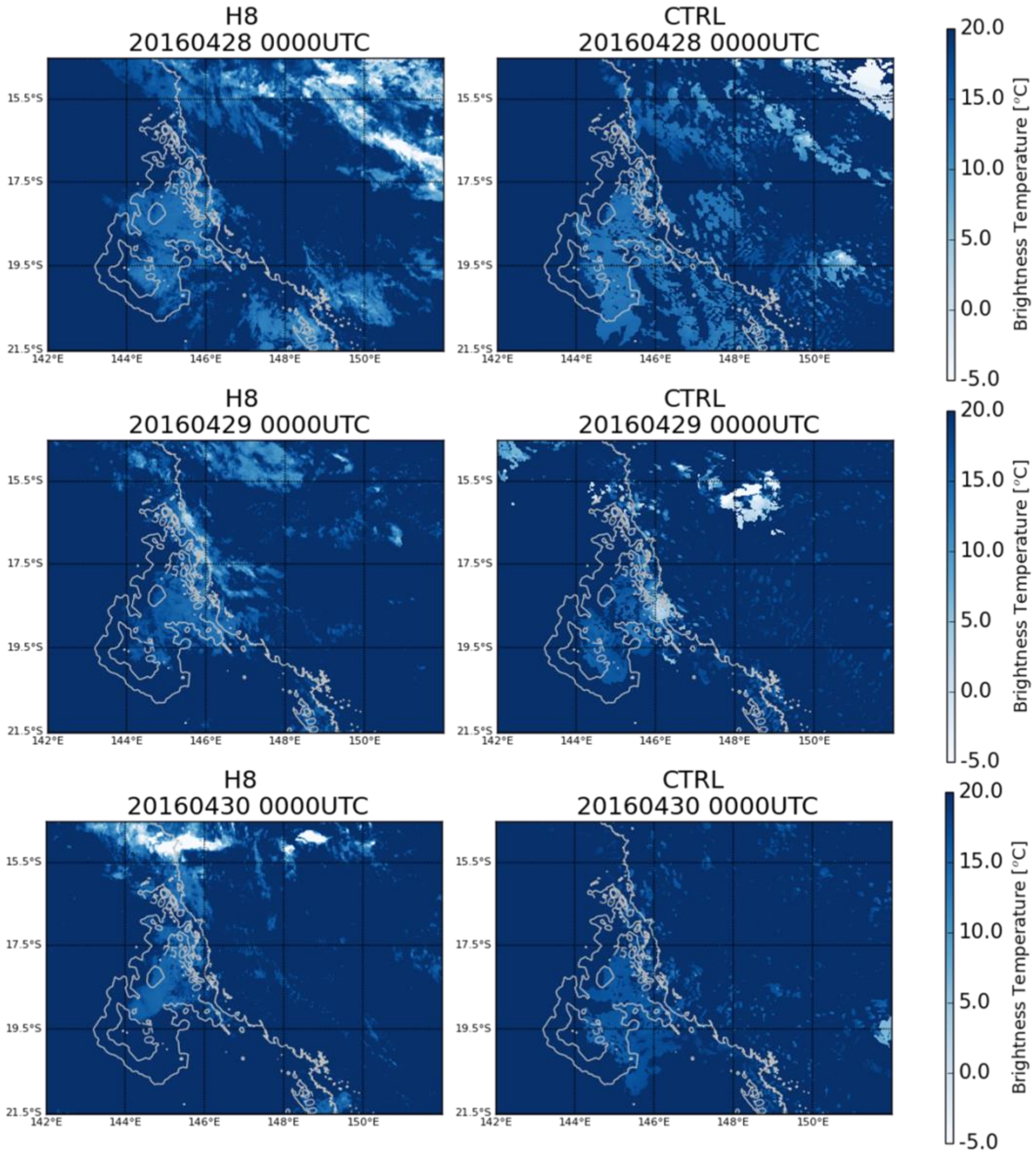

Figure 6: (left) Brightness temperatures of band 13 (10.4 μm) derived from Himawari-8 satellite observations at 0000UTC on 28, 29 and 30 April 2016. (right) Simulated brightness temperatures from CTRL at 3 km resolution at 0000UTC on 28, 29 and 30 April 2016. Note that same color scales applied in all panels. Grey lines denote the coastline and topography map from 500 to 1500 m with 250 m interval.

5 Sensitivity analysis

5.1 Orographic effects

To explore any upwind effect of the orography over the Wet Tropics, two 1° x 1° sub-domains are selected with one covering the primary orographic area (hereafter downwind sub-domain, Figure 3c) where the major precipitation occurs (see Figures 2 and 9a), and another over the upwind water area (hereafter upwind sub-domain, Figure 3d). The simulated cloud fraction (CF) has been analysed over these two sub-domains, respectively. Note that, in the WRF output, CF for each grid point is given by either binary number 1 or 0 to indicate either cloudy or cloud free pixel. In this study, CF of the target domain (e.g. 1°×1° upwind and downwind sub-domains) is defined as the proportion of total grid points in the domain that are classified as cloudy grids for each model level. For each model level from 0.5 to 6 km, the CF is calculated for each hour. Figures 7 and 8 show the 2-dimensional Probability Density Function (PDF) distribution of the CF across the domains for the 60 hours of simulation. To generate the PDF, 100 bins are applied to both variables CF and altitude. Then the probability density for each grid point is calculated based on CF samples at model levels from 60 simulations hours. The uppermost level of this analysis is set to 6 km as most of the clouds are observed to be at low to mid-level during the simulation period. As shown in Figures 7a and 8a, the simulated CF over these sub-domains from CTRL is between 0.5 and 2.5 km (i.e. boundary layer clouds and trade wind cumuli). Note that the boundary layer height over the Wet Tropics is around 950 m in the CTRL run (not shown) and the trade wind inversion base is at around 2 km (see Figure 10a).

Comparing the simulated CF distribution between Topo300 and CTRL runs over the orographic area (Figure 7d), there appears to be a noticeable decrease in cloud cover in the Topo300. The most pronounced reduction (~78%) is evident at lower altitudes, specifically below 2 km. Cloud top height is generally reduced in Topo300, with a greater number of simulation hours in Topo300 indicating a CF near zero above 2km. This same feature is also seen over the upwind coral reef area (Figure 8d), though the magnitude of the CF is relatively small (~40%) compared to the mountain area. Larger differences in CF are, once again, found at lower altitudes (below 2 km). It is interesting to note that the orographic enhancement of the low-level cloud fraction, extending to the eastern water area, potentially provides a sheltered area for the coral reefs, protecting them from severe bleaching through reducing the solar radiation heating (examples of cloud fields are shown in Figure S5). This result is consistent with the observational analysis presented by Zhao et al. (2022), which highlighted a notable increase in the frequency of low-level clouds associated with orographic enhancement in the Wet Tropics.

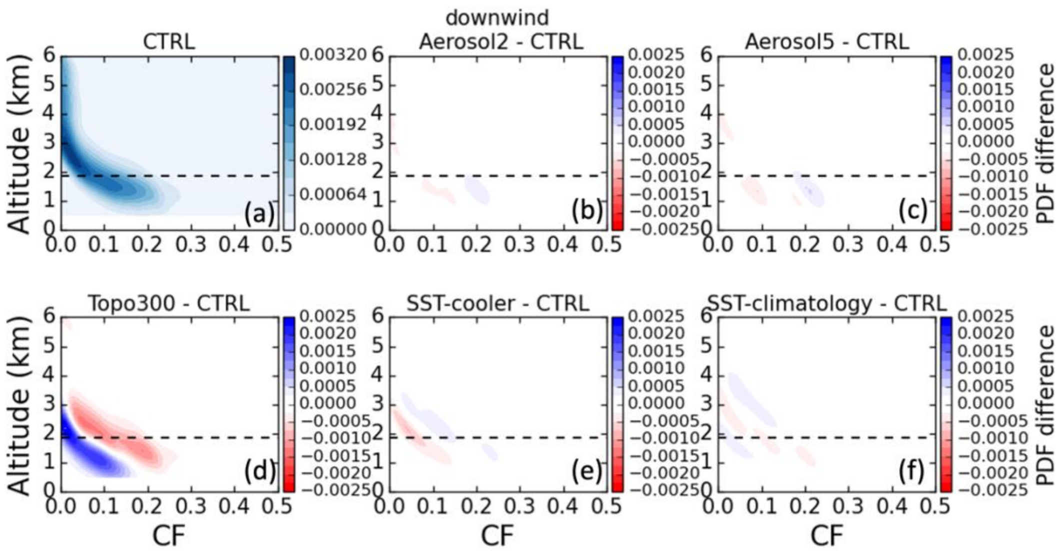

Figure 7: (a) Vertical PDF distribution of 1 km resolution simulated cloud fraction over the downwind mountain area (shown by red square in Figure 3c) from CTRL-run. (b-f) Difference plots between CTRL-run and Aerosol2, Aerosol5, Topo300, SST-cooler, SST-climatology. The analysis is for 60h simulation time after the spin-up from 2016-04-28

0000UTC to 2016-04-30 1200UTC. Note that dashed lines indicate the average base height of TWI over the downwind subdomain.

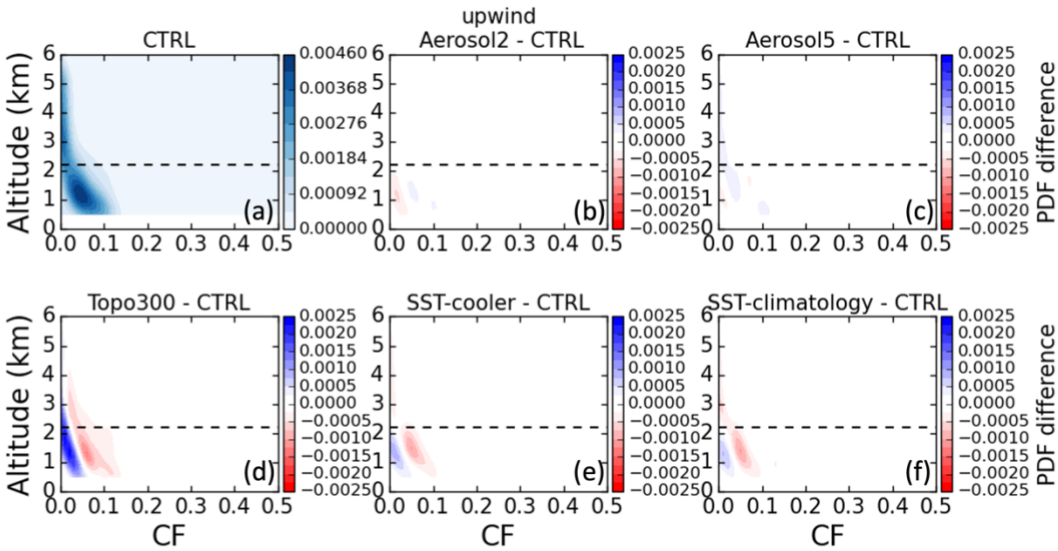

Figure 8: Same as Figure 7, but for the upwind water area (shown by red square in Figure 3d).

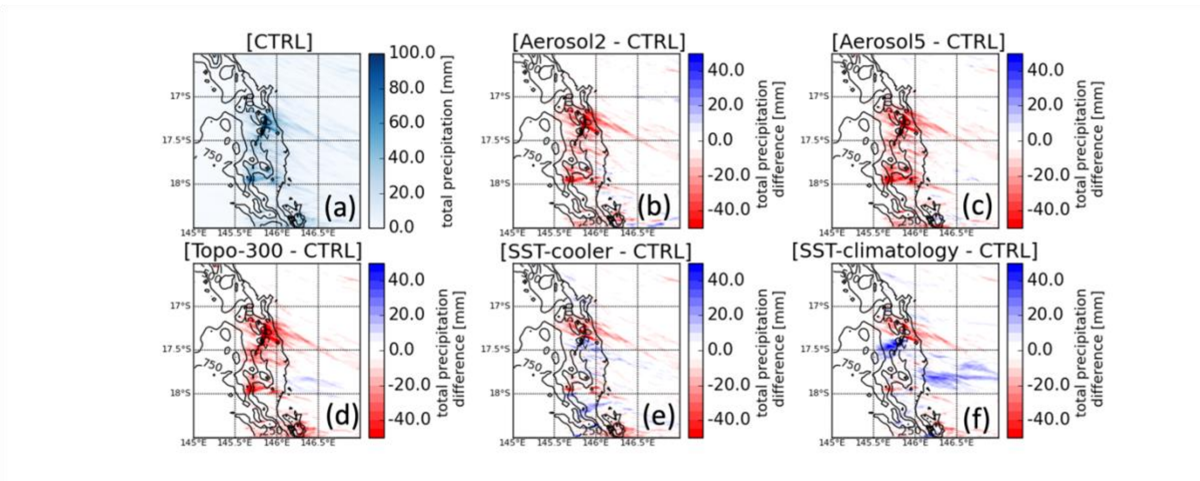

Figure 9: (a) Accumulated precipitation for the time period of 2016-04-28 0000UTC to 2016-04-30 1200UTC from 1 km resolution with CTRL-run. (b-f) Difference plots of accumulated precipitation between CTRL-run and Aerosol2, Aerosol-5, Topo300, SST-cooler, SST-climatology, separately. Black contours indicate the topography map from 250 to 1500 m by 250 m-interval.

Figure 9 shows the map of accumulated precipitation over the inner-most domain from 1 km WRF simulations from the CTRL-run, and the difference between CTRL-run and sensitivity studies, respectively. The accumulation period is the 60-h simulation time after the spin-up (i.e. from 0000UTC 28 to 1200UTC 30 April 2016). As shown in Figure 9d, a strong reduction in precipitation (~44%) over the topography is evident when the topography is modified, particularly over the windward slopes. Over 40 mm difference in the accumulated precipitation is noted at the points of highest precipitation grids between the Topo300 and CTRL simulations, highlighting the major role of terrain in the development of precipitation. In addition to the mountain area, this precipitation reduction has also been seen over the upwind region, extending to the GBR. A slight increase in the accumulated precipitation is noted in the southern part of the upwind domain, indicating the chaotic nature of cloud and precipitation in weakly-forced locations.

The local cloud and precipitation differences shown in Figure 7d, 8d and 9d can be elucidated through the examination of convection-related variables, including convective available potential energy (CAPE), 10 m wind convergence (calculated as (-1) × (∂u/∂x + ∂v/∂y), Schneider et al., 2018) and velocity difference (w_{diff}) between the maximum vertical velocity below the level of free convection (LFC) and the required updraft velocity to overcome convective inhibition (CIN), calculated as $\sqrt{2 \times CIN}$ (Trier 2003). Positive values of w_{diff} indicate that air parcels can reach their respective LFC, release CAPE and initiate convection. Also, simulated trade wind inversion (TWI) properties have been analysed, including its base height, thickness, and strength. This analysis is important because trade-wind cumuli are constrained by the TWI, particularly over the oceanic regions. It is also perhaps more difficult to directly link changes in cloud and precipitation process over the upwind domain to the direct mountain-induced lifting and low-level wind convergence. Additionally, the lower troposphere stability (LTS) and estimated inversion strength (EIS) have been examined, which are good indicators of the changes of low-level cloud (Wood and Bretherton, 2006). LTS is defined as the potential temperature difference between a nominal location in the free troposphere (typically 700 hPa) and the surface. EIS is further developed to obtain a more precise estimate of the strength of the boundary layer inversion by removing the variability of the free tropospheric thermodynamic structure (Wood and Bretherton, 2006), which is defined as $LTS - \Gamma_m^{850}(z_{700} - LCL)$, where Γ_m^{850} is the moist adiabatic potential temperature lapse rate, z_{700} is the altitude of the 700hPa pressure level, and LCL is the lifting condensation level computed using the expression LCL = 125 (T – Td), which is based on the temperature (T) and dew point temperature (Td) at the surface (Lawrence, 2005). Note that all these variables are calculated for each grid point at each hour.

As seen from Figure 10a, a notable increase in CAPE is seen in the Topo300 over the downwind area, whereas only small increases are found at the upwind. This change in CAPE is clearly explained by the change in orography. The atmosphere deepens when the mountains are reduced, leading to higher temperatures at the surface (Figure S6). Because the relative humidity is essentially unchanged, the LFC is lower, which results in higher CAPE values over the topography in the Topo300 experiment. However, fewer grid points are simulated with positive w_{diff} in the Topo300 run over the downwind area (Figure 10c), making the CAPE more challenging to release. This therefore results in a reduced cloud fraction and precipitation in the Topo300, despite the presence of higher CAPE values at the downwind area. Low-level wind convergence over the downwind area is much stronger in the CTRL run, as the lack of strong orographic lifting in the Topo300 run produces only weak low-level convergence. However, this is not as significant over the upwind area, where little to no difference in w_{diff} and low-level convergence is seen between CTRL and Topo300 (Figure 10b-c). There is a notable increase in the stability of the lower troposphere over mountainous regions (Figure 10d), which is largely attributed to the reduced elevation in these areas. A less stable lower troposphere suggested in the CTRL is conducive to the enhanced development of trade cumulus clouds. The comparison of LTS between the CTRL and Topo300 scenarios over the upwind, however, reveals minimal differences, suggesting that the impact of orography on atmospheric stability is predominantly localized.

As expected, the upwind area experiences weaker effects of mountain-induced lifting, and so the impacts of the alteration in mountain height are attenuated. However, changes in topography do lead to modifications in the upwind airstream (Chu et al., 2000; Zhang et al., 2022). Altered upwind temperature and wind profiles are likely to result in modifications of TWI and boundary layer inversion characteristics. It is possible that the height and thickness of trade wind inversion is being modified in the Topo300, which constrains the trade cumulus development over the upwind area. To explore this possibility, we compared the simulated TWI properties and EIS in the CTRL and Topo300 runs (Figure 10e-h). The results show that a higher inversion base height with a relatively larger inversion thickness is present in the CTRL run over both downwind and upwind areas, whereas a reduction in orography results in a lower TWI base height and a smaller inversion thickness over the upwind area. The lower TWI in the Topo300, as a result, constrains the vertical development of the clouds, resulting in a lower cloud top height and less developed cloud and precipitation systems. Interestingly, measures of inversion strength, specifically TWI strength and EIS, exhibit no substantial variation in response to the changes in topography, over both downwind and upwind domain (Figures 10f and h). It is considered that atmospheric inversions strength is often influenced by synoptic to larger-scale atmospheric processes (Milionis and Davies, 2008) which can override the local topographic effects. In contrast, the height of inversion layer might be more influenced by factors such as local topography. To summarize, the vertical velocity and low-level wind convergence, coupled with the TWI, are crucial in explaining the cloud and precipitation features over the downwind area, which can be directly linked to the mountain induced lifting and flow deviation. On the other hand, the upwind effect of orographic enhancement is more closely associated with the alterations in TWI properties, especially the height and thickness of TWI.

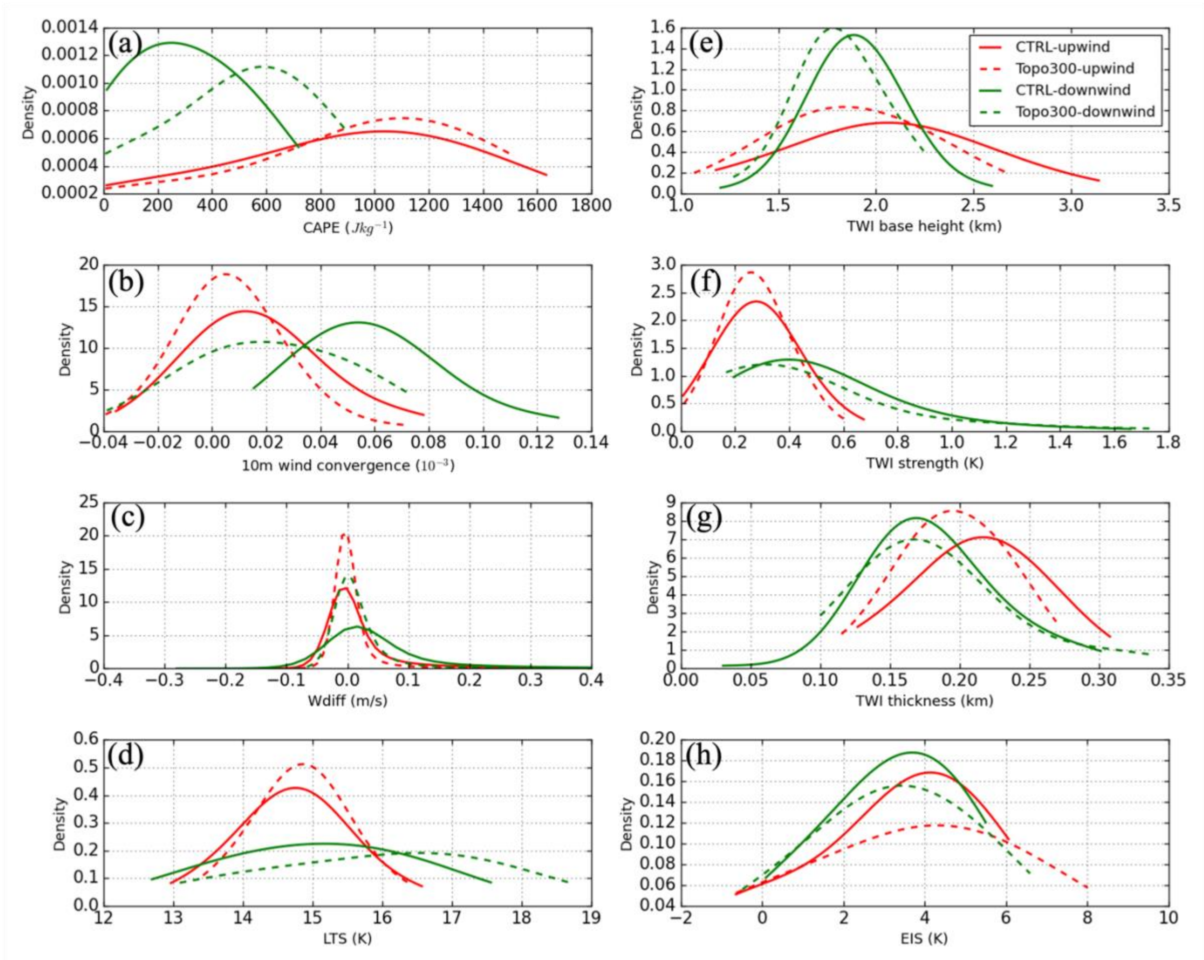

Figure 10: PDF distribution of the (a) CAPE, (b) low-level wind convergence, (c) W_{diff}, (d) LTS, (e) trade inversion base height, (f) inversion strength, (g) inversion thickness, and (h) EIS over the upwind (red lines) and downwind (green lines) area, separately. The analysis covers the whole 60 h simulation period after the spin-up time. Solid lines represent results from CTRL, and dashed lines are for Topo300 sensitivity experiment.

5.2 Local aerosol loading

We have also explored the hypothesis that regional aerosol loading may affect the cloud and precipitation properties over the GBR. As shown in Figure 11a, doubling the surface WFA emission over the GBR (Aerosol2 experiment) results in an increase of ~700/cm^3 (~122% increase) in the near-surface WFA number concentration over the upwind sub-domain (from 572/cm^3 to 1250/cm^3), throughout the evolution of the simulation. The increase in WFA emission at the surface also leads to an increase in the atmospheric WFA population to levels above 2 km (Figure 13a). Pertaining to the Aerosol5 experiment, the near-surface WFA number concentration increases by approximately 1400/cm^3 (~251% increase), from 572/cm^3 to 2241/cm^3, in comparison to the CTRL (Figure 11a) as well as an enhancement in the upper-level profile of the WFA concentration (Figure 13e). A slight time-variation in WFA number concentration (WFANC) is seen for both Aerosol2 and Aerosol5, which primarily results from the advection and diffusion of the aerosol during the model integration (Thompson and Eidhammer, 2014). The gradual increase of the WFA number concentration during the last day of the simulation is primarily attributed to the strong inflow with an additional significant amount of aerosols from the southern portion of the GBR when the surface wind changes from easterly to southeasterly (Figure 4). It is worth noting that a fairly similar increase in the WFANC is also seen over the downwind subdomain in both Aerosol sensitivity experiments (Figures 12a, 13a, and 13e). Given the predominance of trade wind patterns in this region, this downwind impact is not unexpected.

Cloud droplet number concentration (CDNC), considered both upwind and downwind, is sensitive to the changes in the atmospheric aerosol number concentration (Figures 11b and 12b). A higher CDNC corresponding to an increase in the WFA population is evident from the cloud base to the cloud top (Figures 13b and 13f), which is consistent with the findings presented in Fiddes et al. (2022). Total CF, however, is found to be essentially unaffected by the changes in the aerosol concentration over both sub-domains (Figures 11c and 12c). The vertical profile of CF over the upwind subdomain (Figure 13c) suggests a slight deepening of the trade cumulus with an increase in domain-averaged CF at cloud top, especially in Aerosol5 experiment (also shown in Figure 8c). Minimal response is seen at cloud base. This is consistent with an increase of the liquid water path (LWP), which is evident in both the Aerosol2 and Aerosol5 experiments (Figures 11d and 13d) over the upwind. Looking downwind, even though the CF remains largely unchanged across the altitudes (Figures 13g, 7b and 7c), a cloudy layer with higher CDNC could also result in a larger LWP, that is likely due to cloud lifetime effects (Albrecht 1989; Zhang et al., 2016), as shown in Figure 12d. Additionally, the cloud radiative effect (CRE) has been considered through the CTRL run and the Aerosol sensitivity experiments. CRE is defined as the net radiation flux (downward flux minus upward flux) under all sky conditions minus the net radiation flux under clear sky conditions and can be applied to both the surface and top of atmosphere (Imre et al., 1996; Bao et al., 2020). Here, in this analysis, it focuses on the shortwave CRE (SWCRE) at the surface, as it represents the effective solar heating of the sea surface. As shown in Figures 11e and 12e, a rise in SWCRE, though small with a maximum of 50 W/m^2, is evident with increase in aerosol population over both sub-domains. This is primarily attributed to the higher CDNC, as the cloud reflectance is enhanced with increased droplets number concentration.

As shown in Figures 9b and 9c, a reduction in total precipitation is seen in both Aerosol sensitivity experiments, primarily over the downwind mountain area, with a maximum 30mm difference (~30% reduction) noted around the peak precipitation points. This decreased precipitation is evident throughout the simulation hours between the CTRL and Aerosol sensitivity runs (Figure 12f). Relatively small changes (less than 20 mm) in accumulated precipitation are seen over the upwind area, where the decreased accumulated precipitation mainly originates from a few hours in the last day of simulation (Figure 11f). Although small in magnitude, the warm cloud precipitation over the GBR is found to show considerable responses to the changes in the local aerosol loading.

Increased CCN concentrations can be expected to produce smaller droplets for a given liquid water content (Twomey, 1997). The smaller cloud droplets can reduce the efficiency of collision and coalescence, which may inhibit precipitation development (Albrecht, 1989). Over the GBR, sensitivity experiment in this study indicates consistently that, cloud microphysical properties, including CDNC and LWP, and precipitation respond strongly to changes in the local WFANC. A significant rise in CDNC (~2.5X in Aerosol5) is correlated with an increase in the aerosol population is seen over the GBR, and predominantly leads to suppressed precipitation (up to a 40mm reduction in total precipitation) over both upwind and downwind areas. While the total CF is showing less sensitivity to the aerosol perturbations. It's worth noting that the Aerosol sensitivity experiments also show evidence of deepened trade cumulus over the upwind region, which will increase the LWP and the SWCRE. Note that fluctuations in LWP response are observed throughout the simulation. Previous studies have shown that multiple processes (e.g. cloud formation processes, evaporation, and precipitation) play a role in determining the LWP response to aerosol perturbations (Han et al., 2002). Also, meteorological conditions (e.g. relative humidity) could strongly modulate the LWP-droplet number concentration relationship (Gryspeerdt et al., 2019). A notable downwind effect featured by a significant reduction of surface precipitation is simulated when changing the surface aerosol emissions over the GBR.

It should be noted that how convection may interact with changes in aerosol is still a large source of uncertainty (Tao et al., 2012) and experiments in this study only focus on perturbing the water friendly aerosol loading over the GBR. Previous studies have shown that the thermodynamic environment is strongly modulated by the large-scale forcing, whose impact on the cloud field might surpass that of local aerosol perturbations (Dagan et al., 2018; Spill et al., 2021). Spill et al. (2021) show that the response of cumulus cloud and precipitation to the aerosol perturbation is much stronger in the idealised simulations without the large-scale forcing. This suggests a potentially limited effect of aerosols on cumulus cloud fields in the realistic condition due to the predominant influence of large-scale forcing. The nature variability of the marine shallow clouds and precipitation process could also explain some of the differences between the CTRL and Aerosol sensitivity runs.

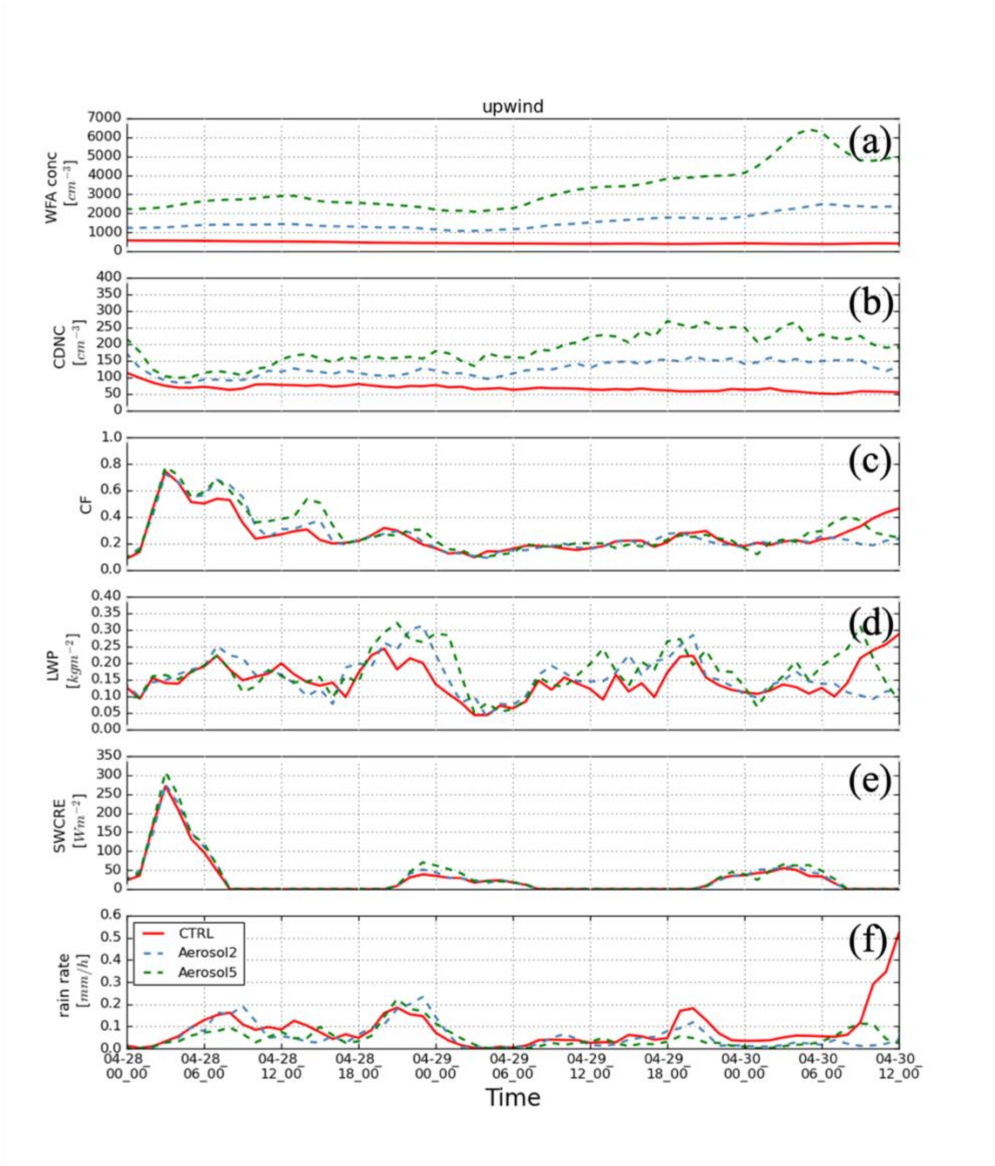

Figure 11: Time series of domain-averaged (a) water-friendly aerosol number concentration, (b) cloud droplet number concentration, (c) cloud fraction, (d) liquid water path, (e) shortwave cloud radiative effect, and (f) rain rate from 1 km resolution with CTRL (red solid lines), Aerosol2 (blue dashed lines), and Aerosol5 (green dashed lines). The target area is over upwind sub-domain.

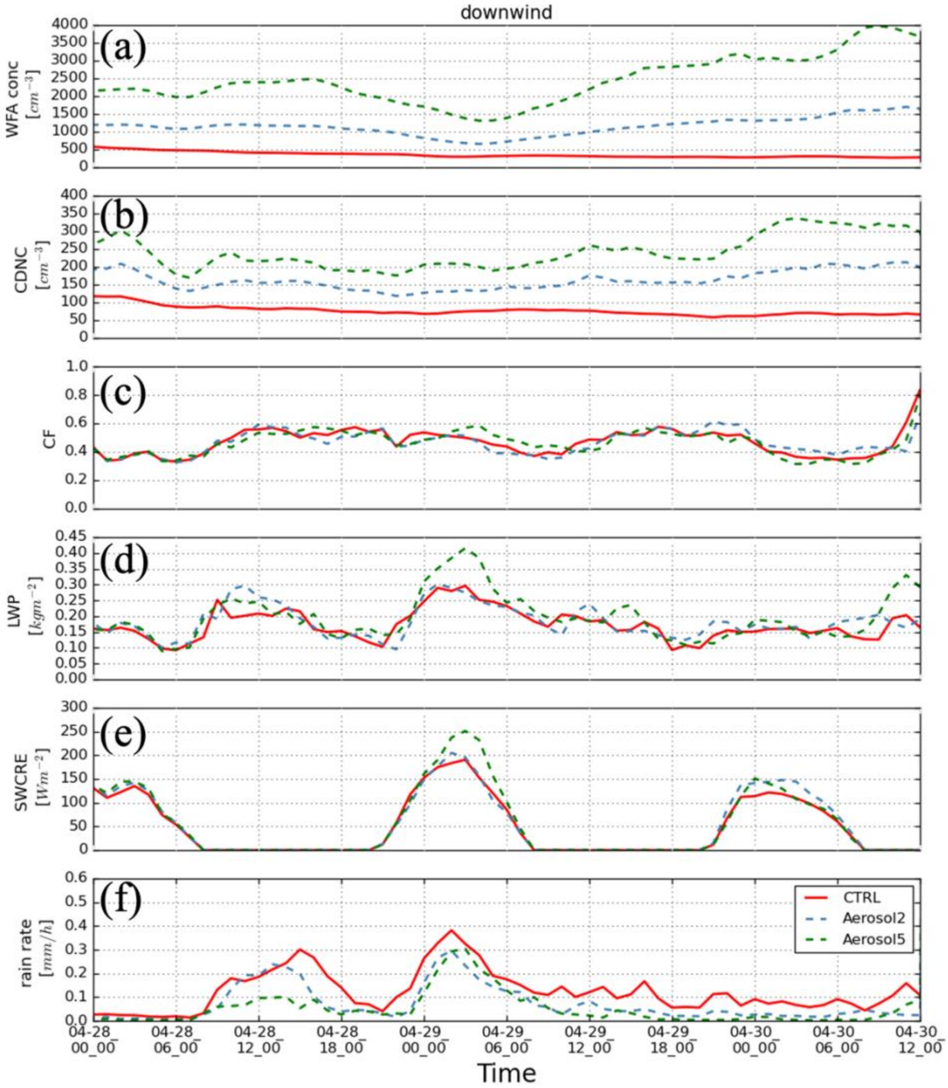

512

513 **Figure 12: Same as Figure 11, but for downwind sub-domain.**

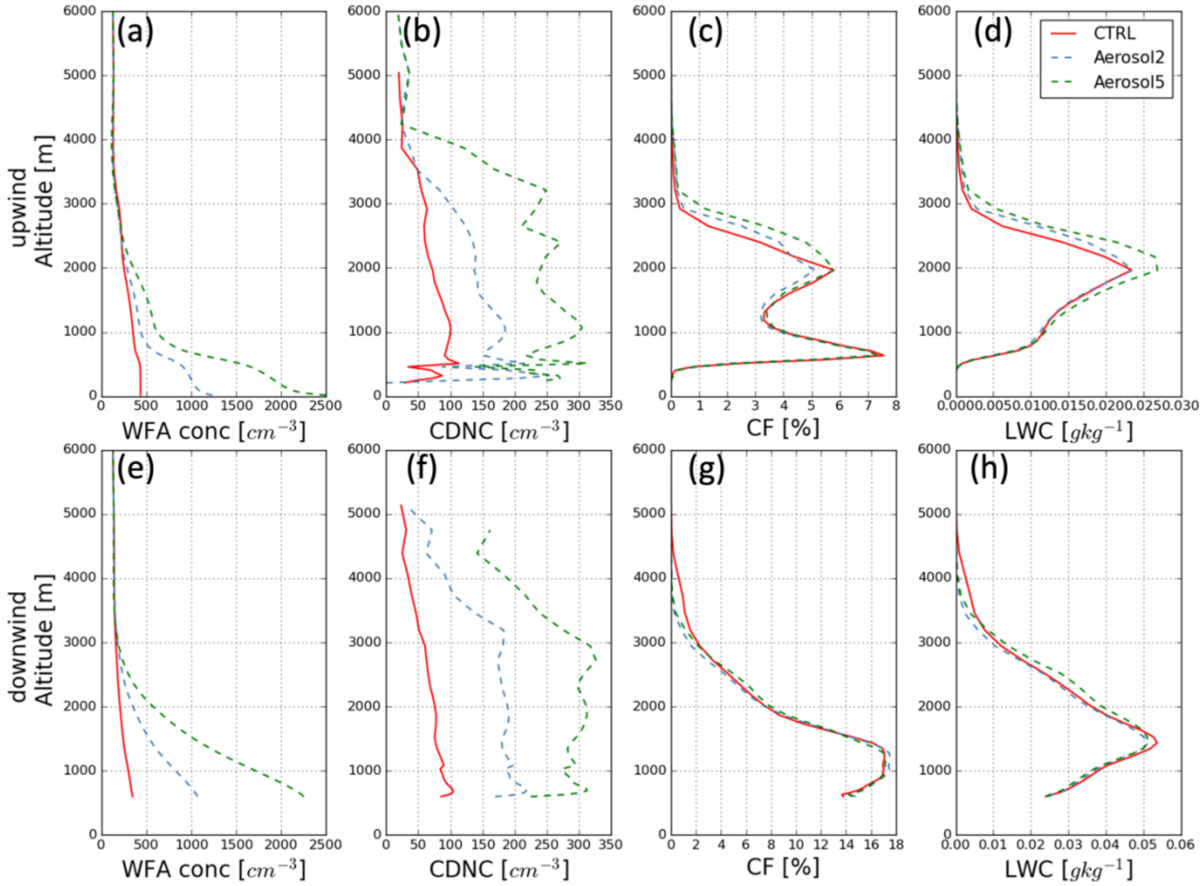

Figure 13: Vertical profiles of (a) domain-averaged water-friendly aerosol number concentration, (b) in-cloud averaged cloud droplet number concentration, (c) domain-averaged cloud fraction, and (d) domain-averaged liquid water content over the upwind sub-domain from CTRL (in red), Aerosol2 (in blue), and Aerosol5 (in green). The analysis is for 60h simulation time after the spin-up from 2016-04-28 0000UTC to 2016-04-30 1200UTC. (e-h) same as (a-d), but for downwind sub-domain.

5.3 Local SST forcing

In this section, it has explored the sensitivity of cloud and precipitation properties over the GBR in response to the local SST changes. A reduction in CF is noted over the upwind in the SST-cooler run, with the most notable difference apparent at lower altitudes (Figure 8e). Over the downwind sub-domain, the CF has only a small difference between the CTRL and SST-cooler experiments (Figure 7e). However, a decrease in the accumulated precipitation is discernible over downwind points with the peak accumulated precipitation (Figure 9e). Similar but more variable findings are evident from the SST-climatology experiment. Figure 7f shows small but more complex changes in CF in the downwind area with associated positive and negative changes in accumulated precipitation (Figure 9f). These variable impacts are likely due to the non-uniform (positive and negative) changes in SST associated with the differences between the CTRL and SST-climatology runs. (Figure S1). The downwind effect on precipitation is similarly discernible in the SST-climatology, however there are no noteworthy results related to the cloud fraction (Figure 7f).

Theoretically, a warmer SST will likely provide more water vapor in the atmosphere through increased surface latent heat fluxes (Rieck et al., 2012; Vogel et al., 2016). The increased atmospheric water vapor, under such conditions, will consequently induce more rainfall at local and downstream regions. A decrease in surface heat flux and moisture flux is noted in the SST-cooler experiment (Figure 14), preventing the formation and development of the shallow cloud. There is a relative minor difference in averaged surface flux between the CTRL and the SST-climatology experiment (Figure 14), that is potentially associated with non-uniform modifications in SST (Figure S1). However, a notable wide distribution of surface flux is likely contributing to the complex response of cloud and precipitation in the SST-climatology (Figures 7f and 9f). It is also suggested that with a warmer SST, the boundary layer becomes more humid, which becomes destabilized by increased clear-sky radiative cooling, driving more cumulus convection (Narenpitak and Bretherton, 2019; Wyant et al., 2009; Narenpitak et al., 2017). In this study, the SST-cooler experiment reveals a more stable lower troposphere (Figure 15a) compared to CTRL, which inhibits the formation of trade wind clouds. A slight unstable condition is seen in the SST-climatology experiment, which is likely contributed to the warmer pool at the upwind ocean, driving a more variable changes in cloud and precipitation (Figures 7f and 9f). Another factor that controls the cloud amount is the free tropospheric humidity (Bretherton et al., 2013; Eastman & Wood, 2018). It is suggested that drier air at the level of free troposphere causes more entrainment drying, depleting the boundary layer cloud water. As shown in Figure 15b, slightly drier condition is seen at the lower level below 1km in the SST-cooler, however, there is no significant difference near the free troposphere (2.5km). Large-scale circulation as well as local processes play important role in driving the thermodynamic profiles (Nygård et al., 2021). Considering the magnitude of adjustment in surface temperature, the changes may not be felt by the upper atmospheric levels. This limited impact could be further diminished by large-scale atmospheric dynamics. Nevertheless, drier condition at lower level is likely contributing to the stabilized boundary layer simulated in the SST-cooler experiment. Finally, two measures of the inversion strength, specifically TWI strength and EIS, have been examined with SST experiment. The results show that inversion strength is not a predominant factor impacting the interactions of trade clouds and local SST forcing. As discussed above, the inversion strength is more likely to be influenced by synoptic to larger-scale atmospheric processes (Milionis and Davies, 2008), which have the potential to eclipse the impact of local forcings.

Over the tropics, the SST has been noted in several studies to be a key factor controlling the location of rainfall over various timescales (Lu and Lu, 2014; Jo et al., 2019; Wu et al., 2009; Wu and Kirtman, 2007). Takahashi and Dado (2018) highlight the impact of local and/or nearby SST on local and regional climate. In particular, they found that warmer local SST results in greater rainfall over the downstream land region in the mid-latitudes based on observational dataset, which suggests strong air-sea coupling processes. Numerical sensitivity experiments in this study, to some extent, show consistent results, indicating that precipitation over the GBR shows response to the underlying SST conditions, though the effect is weak on the scales considered here. A downwind effect on the precipitation has been found over the Wet Tropics. Sensitivity of cloud fraction in response to SST variation is seen over the water area, though the magnitude is minor in comparison with the major orographic impacts. The relationship between cloud fraction and SST at the lower levels have been found to largely depend on the type of cloud and its height (Cesana et al., 2019). A stronger response of "lower-top" shallow cloud properties (i.e.

stratocumulus) to the changes in SST is noted in Cesana et al. (2019) in comparison with "higher-top" shallow clouds, for example, cumulus. As such, much minor responses to the changes in SST are expected when considering cloud fields with the higher cloud tops. In this study, instances of simulated cloud field with cloud tops over 3km could largely contribute to the variety of the responses to SST forcing.

Overall, simulations in this study suggest that warm-cloud precipitation over the GBR is sensitive to the underlying local SST forcing, though the responses are weak on the scales considered in this study. The lower troposphere stability and surface heat and moisture flux primarily likely explain most of the responses of trade cumulus over the GBR to local SST forcing. This work supports the important role of local SST on the regional climate over the GBR, but further work on understanding the synoptic and thermodynamic background and air-sea coupling processes is necessary to help elucidate the mechanisms involved.

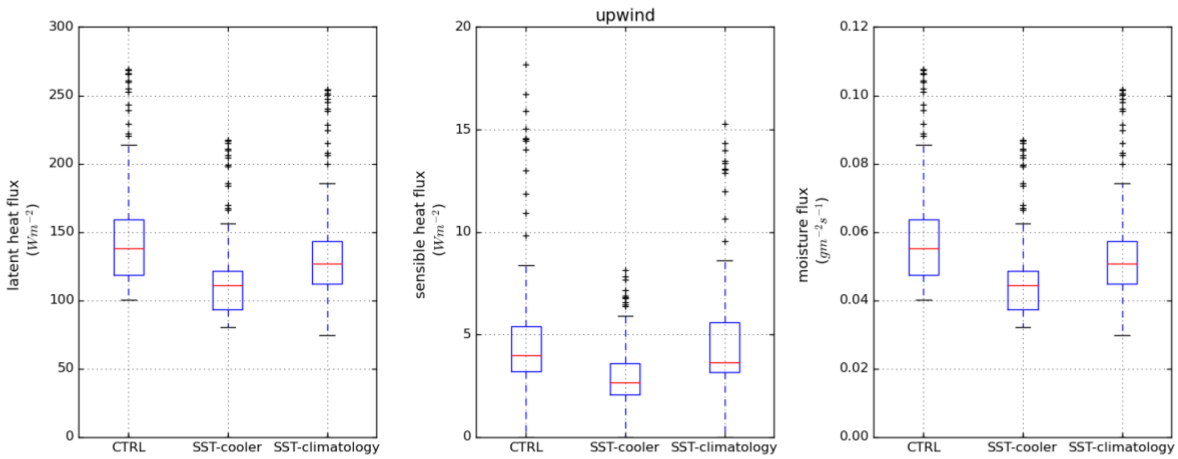

Figure 14: Boxplots showing the comparison of latent heat flux, sensible heat flux, and moisture flux from 1 km resolution simulation with CTRL, SST-cooler, and SST-climatology. The analysis is for 60h simulation period, and over the upwind sub-domain.

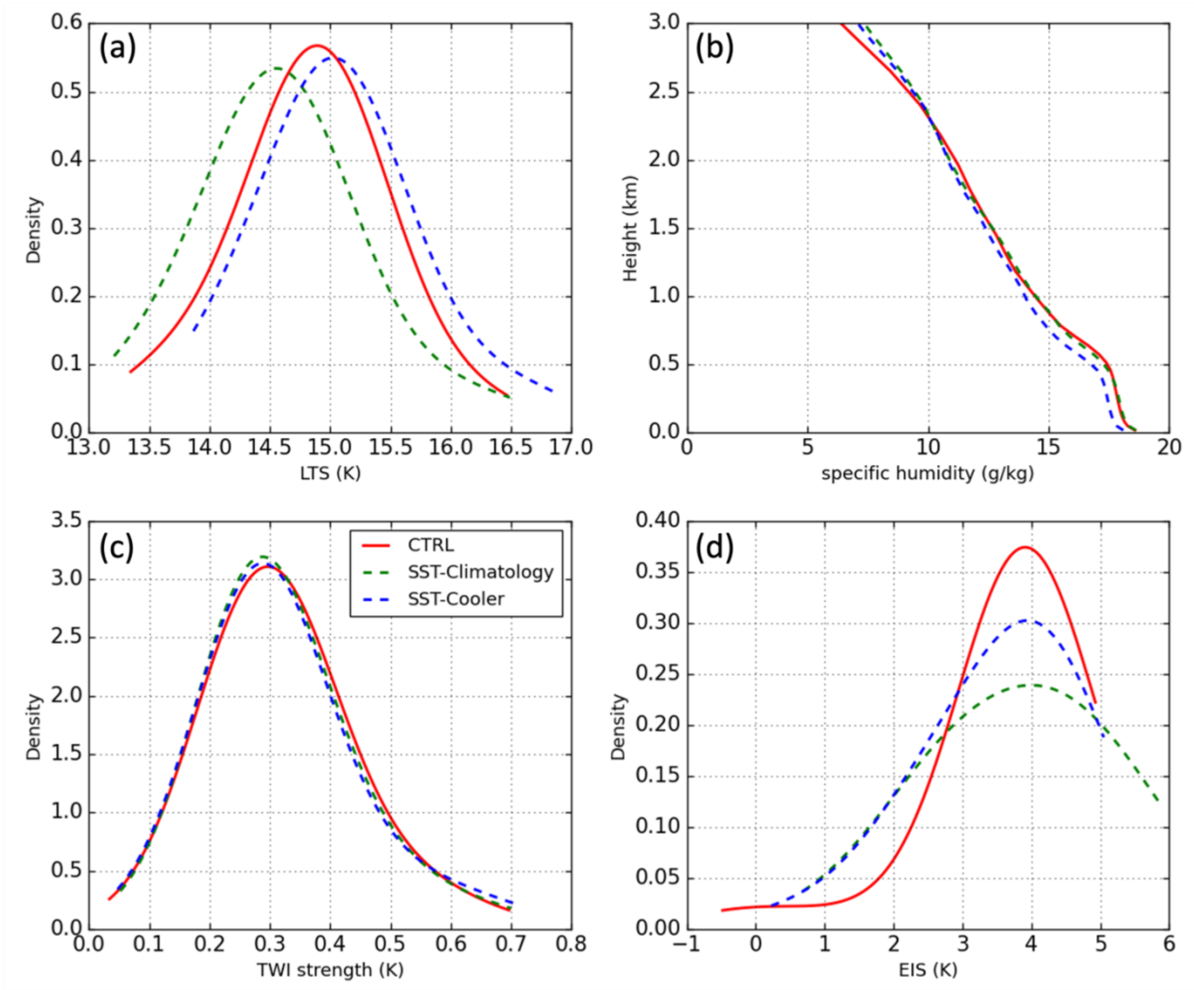

Figure 15: PDF distribution of the (a) LTS, (b) vertical profile of humidity, (c) TWI strength, and (d) EIS over the upwind area. The analysis covers the whole 60 h simulation period after the spin-up time. Red solid lines represent results from CTRL, and dashed lines are for SST sensitivity experiments.

6 Summary and conclusions

A primary aim of this research is to study the sensitivity of trade cumulus precipitation to different local forcings over the GBR using a case study of an orographic precipitation event associated with low-level trade cumulus at the end of April 2016. The selected days for the simulations are characterised by well-defined cumulus and stratocumulus under the trade wind regime without any overlying high clouds. These trade cumuli are observed to generate precipitation over the Wet Tropics around Townsville.

The large-scale meteorology is well captured in the CTRL simulation in terms of the location, duration and magnitude of the surface pressure system and wind fields. Comparison of the upper air profiles from both Townsville and Wills Island sounding stations showed good agreement in wind speed, wind direction and temperature profiles. The CTRL simulation also demonstrated a considerable level of skill in simulating both the spatial distribution and the intensity of precipitation over the Wet Tropics as compared to ground observations.

Sensitivity experiments are conducted to investigate the sensitivity of trade cumulus and precipitation in response to the local forcings. Major findings from the sensitivity analysis presented in this study are summarized as follows:

- Reducing the elevation above 300m by 75% decreases the cloud fraction and accumulated precipitation over the Wet Tropics, including both downwind and upwind areas. Weaker vertical velocity, low-level wind convergence and more stable lower troposphere are generated in the Topo300 run over the downwind sub-domain, suggesting their crucial role in rainfall production. The reduced TWI base height in the Topo300 run is found to limit the cloud-precipitation development over the upwind water area.
- Cloud microphysical properties, including CDNC, LWP, and precipitation are sensitive to the changes in atmospheric aerosol population over the GBR. Higher CDNC and LWP correlated to increased aerosol number concentration leads to a rise in SWCRE, though the magnitude is small, over both sub-domains. Although CF remains largely unchanged, a deepened cloud is evident over the upwind when WFANC is increased. A downwind effect on cloud and precipitation properties is further noted.
- Cloud fraction and total precipitation over the GBR show a small response to the underlying local SST forcing. A reduction in cloud fraction is noted over the upwind water area when the initial SST is reduced, but any difference is negligible over the downstream orographic region. There is a decrease in the accumulated precipitation in the SST sensitivity experiments over downwind girds where the peak accumulated precipitation generated. These small decreases in cloud fraction and accumulated precipitation are likely associated with the consistently decreased surface flux and stabilized lower troposphere in the SST experiments.

It should be noted that a limitation of this present study is the choice of model set-up in relation to the aerosol representation. In this work, the microphysics scheme simply treats aerosol categories into 'water friendly' and 'ice friendly'. While using a more comprehensive representation of aerosol sources in the model is desirable for a more complete understanding of the complex interactions between aerosols and atmospheric processes (Ghan et al., 2012; Wang et al., 2013), these aerosol-resolving models commonly come at a significant computational cost and are simply unaffordable at a cloud-resolving resolution over a large domain. The primary aim of this study is to better understand the first-order impacts of local forcings on the clouds and precipitation over the GBR, which is the first step towards a more comprehensive investigation of aerosol-cloud-climate interactions. This research requires a large domain at reasonably high resolution to properly capture the complex interactions between the large-scale meteorology and local forcings, which are critical for trade-wind cloud formation (e.g. Vogel et al., 2020; Bretherton and Blossey, 2017). Although far from perfect, the use of the (simplified) aerosol-aware Thompson and Eidhammer (2014) scheme in a convection-permitting configuration is a reasonable middle ground to address these two critical needs. Note that a combination of sulfates, sea salts, and organic matter is found to represent a significant fraction of known CCN and are found in abundance in clouds worldwide (Thompson and Eidhammer, 2014). Therefore, while it would be an interesting (and important) topic for a different project, a precise understanding of aerosol sources, amounts and composition is beyond the scope of the present study.

It might be considered desirable to employ the higher-resolution modelling such as large-eddy simulation (LES) to better resolve the details of the complex cloud and precipitation processes. Although simulations in this study are at a lower resolution than needed to resolve detailed cloud processes such as entrainment and convective aggregation, they are at a high enough resolution to explicitly represent convection while allowing for a considerably larger domain size at an affordable computational cost. The significance of a large domain size has been demonstrated in accurately representing the mesoscale organization of trade-wind cumulus (Vogel et al., 2020; Bretherton and Blossey, 2017). High-resolution LES is not currently possible at the larger domain sizes considered in this study, and therefore it is difficult to use it to study detailed interactions between orography, cloud organisation and variation, and large-scale forgings. In addition, it is acknowledged that presenting statistical significance values is inherently challenging in case studies due to the unique nature of each case and limited samples. However, it is believed that the careful consideration of the model's set-up, combined with a thorough comparative analysis, allows this study to present the findings with a reasoned level of confidence.

Although a range of responses of cloud and precipitation to the local forcings are produced across the GBR in simulations presented in this study, it is recognised that ensemble analysis is necessary in the future to better represent the natural variability of these trade clouds and precipitation properties. Subsequent research endeavours should also consider the influence of additional local forcings, such as wind shear (Yamaguchi et al., 2019), in the modulation of cloud and precipitation dynamics within trade wind regimes. Li et al. (2014) also suggests that downdrafts at the cold pool boundary play an important role in the development of trade wind cumuli. These studies highlight the complex nature of atmospheric dynamics in trade wind cumuli and emphasize the necessity of comprehensive investigations into these additional variables to enhance our understanding of cloud and precipitation in trade-wind cumuli in the GBR region. In situ observations will also be necessary to help investigate the detailed lifecycle of these low-level clouds and the development of the topographic precipitation. Furthermore, there is a need to carry out case studies during the time of intense SST increases that may induce thermal coral bleaching over the GBR. Nevertheless, this analysis sheds some light on understanding the interactions between trade wind cumuli and local forcings across the GBR and Wet Tropics, where the importance of the local low-level cloud in thermal coral bleaching has recently been identified. This study also holds significant relevance for assessing the comprehensive effects of proposed climate intervention techniques, such as marine cloud brightening, on the thermal balance of the GBR region. While this study provides specific insights into the sensitivity of trade cumulus precipitation over the GBR in a particular time frame, its methodologies and findings have broader applications. It offers valuable insights that can be extrapolated to other regions characterized by pristine trade wind and trade-cumulus conditions, contributing to a more comprehensive understanding of regional climate dynamics.

Data availability statement

All data sets used in this study are freely and publicly available online and may be accessed directly as follows. The University of Wyoming upper-air sounding is downloaded from http://weather.uwyo.edu/upperair/sounding.html. The ERA5 reanalysis data is available at the website: https://cds.climate.copernicus.eu/cdsapp#!/search?-type=dataset. The Australian Bureau of Meteorology Daily rainfall can be downloaded from the website: http://www.bom.gov.au/climate/data/index.shtml. The Himawari-8 full disk observational products are available at NCI THREDDS Data Server: https://dapds00.nci.org.au/thredds/catalogs/ra22/satellite-products/arc/obs/himawari-ahi/fldk/fldk.html. The Himawari-8 true color imagery and cloud types classification are available at JAXA Himawari Monitor supplied by P-Tree System: https://www.eorc.jaxa.jp/ptree/.

Author contribution: W.Z., Y.H., S.S. and M.M. developed the ideas and designed the study. W.Z. collected the data, performed the analysis and prepared the draft manuscript. Y.H., S.S., M.M. and D.H. supervised and reviewed the manuscript. All authors made substantial contributions to this work and approved the final version of the manuscript.

Competing Interests: Some authors are members of the editorial board of journal Atmospheric Chemistry and Physics. The peer-review process was guided by an independent editor, and the authors have also no other competing interests to declare.

Acknowledgements: This work is supported by Reef Restoration and Adaptation Program which is funded by the partnership between the Australian Governments Reef Trust and the Great Barrier Reef Foundation. Wenhui Zhao was also supported by Monash Graduate scholarship while working at Monash University. Yi Huang, and Steve Siems are further supported by Australian Research Council Discovery Grant (ARC DP230100639). The Australian National Computational Infrastructure is also thanked for providing the computational resources. We have also benefited from discussions with Greg Thompson. The authors would like to acknowledge the Traditional Owners of the Great Barrier Reef, particularly the Wulgurukaba and Bindal people of the Townsville region nearby the area of our case study.

References

Albrecht, B. A.: A model study of downstream variations of the thermodynamic structure of the trade winds. Tellus A, 36 (2), 187–202, 1984.

Albrecht, B. A.: Aerosols, cloud microphysics, and fractional cloudiness. Science, 245(4923), 1227–1230. https://doi.org/10.1126/ science.245.4923.1227, 1989.

Bao, Shanhu, Letu, Husi, Zhao, Jun, Lei, Yonghui, Zhao, Chuanfeng, Li, Jiming, Tana, Gegen, Liu, Chao, Guo, Enliang, Zhang, Jie, He, Jie, and Bao, Yuhai: Spatiotemporal distributions of cloud radiative forcing and response to cloud parameters over the Mongolian Plateau during 2003–2017. International Journal of Climatology, 40(9), 4082–4101. https://doi.org/10.1002/joc.6444, 2020.

Berkelmans, R., G. De'ath, S. Kininmonth, and W. J. Skirving: A comparison of the 1998 and 2002 coral bleaching events on the Great Barrier Reef: Spatial correlation, patterns and predictions, Coral Reefs, 23, 74 – 83. https://doi.org/10.1007/s00338-003- 0353-y, 2004.

Bonell, M. and D. Gilmour: Variations in short-term rainfall intensity in relation to synoptic climatological aspect of the humid tropical northeast Queensland coast. Singapore Journal of Tropical Geography, 1 (2), 16–30, 1980.

Bony, S., Dufresne, J.-L., Le Treut, H., Morcrette, J.-J. and Senior, C.: On dynamic and thermodynamic components of cloud changes. Climate Dynamics, 22(2–3), 71–86. https:// doi.org/10.1007/s00382-003-0369-6, 2004.

Boucher, O., D. Randall, P. Artaxo, C. Bretherton, G. Feingold, P. Forster, V.-M. Kerminen, Y. Kondo, H. Liao, U. Lohmann, P. Rasch, S.K. Satheesh, S. Sherwood, B. Stevens and X.Y. Zhang: Clouds and Aerosols. In: Climate Change 2013: The Physical Science Basis. Contribution of Working Group I to the Fifth Assessment Report of the Intergovernmental Panel on Climate Change (IPCC), Cambridge University Press, Cambridge, vol 5, pp 571–657, 2013.

Bretherton, C. S., Blossey, P. N., & Jones, C. R.: Mechanisms of marine low cloud sensitivity to idealized climate perturbations: A single-LES exploration extending the CGILS cases. Journal of Advances in Modeling Earth Systems, 5, 316–337. https://doi.org/10.1002/jame.20019. 2013.

Bretherton, C. S., & Blossey, P. N.: Understanding mesoscale aggregation of shallow cumulus convection using large-eddy simulation. Journal of Advances in Modeling Earth Systems, 9(8), 2798–2821. https://doi.org/10.1002/2017MS000981. 2017.

Bureau of Meteorology: Himawari 8/9 Full Disk Observations – Archive (ARC) data stream. NCI Australia. (Dataset) https://dx.doi.org/10.25914/61a609aa1434d, 2021.

Colarco, P., A. da Silva, M. Chin, and T. Diehl: Online simulations of global aerosol distributions in the NASA GEOS-4 model and comparisons to satellite and ground-based aerosol optical depth. J. Geophys. Res., 115, D14207, doi:10.1029/2009JD012820, 2010.

Cesana, G., Del Genio, A.D., Ackerman, A.S., Kelley, M., Elsaesser, G., Fridlind, A.M., Cheng, Y. and Yao, M.S.: Evaluating 'odels' response of tropical low clouds to SST forcings using CALIPSO observations. Atmospheric Chemistry and Physics, 19(5), pp.2813-2832, https://doi.org/10.5194/acp-19-2813-2019, 2019.

Chen, F., and J. Dudhia: Coupling an advanced landsurface/hydrology model with the Penn State/NCAR MM5 modeling system. Part I: Model description and implementation. Mon. Wea. Rev., 129, 569–585, doi: 10.1175/1520- 0493(2001)1292.0.CO;2, 2001.

Chen, T., W. B. Rossow, and Y. C. Zhang: Radiative effects of cloud-type variations, J. Clim., 13, 264-286, https://doi.org/10.1175/1520-0442(2000)013<0264:REOCTV>2.0.CO;2, 2000.

Chin, M., and Coauthors: Tropospheric aerosol optical thick- ness from the GOCART model and comparisons with satellite and sun photometer measurements. J. Atmos. Sci., 59, 461–483, doi:10.1175/1520-0469(2002)059,0461:TAOTFT.2.0.CO;2. 2002.

Chu, C. M., and Lin, Y. L.: Effects of orography on the generation and propagation of mesoscale convective systems in a two-dimensional conditionally unstable flow. Journal of the atmospheric sciences, 57(23), 3817-3837, https://doi.org/10.1175/1520-0469(2001)057<3817:EOOOTG>2.0.CO;2, 2000.

Colarco, P., A. da Silva, M. Chin, and T. Diehl: Online simulations of global aerosol distributions in the NASA GEOS-4 model and comparisons to satellite and ground-based aerosol optical depth. J. Geophys. Res., 115, D14207, doi:10.1029/2009JD012820, 2010.

Colle, B.A., Wolfe, J.B., Steenburgh, W.J., Kingsmill, D.E., Cox, J.A.W., and Shafer, J.C.: High-resolution simulations and microphysical validation of an orographic precipitation Event over the Wasatch Mountains during IPEX IOP3. Mon. Weather Rev. 133, 2947–2971. https://doi.org/10.1175/MWR3017.1, 2005.

Crook, N. A.: Sensitivity of moist convection forced by boundary layer processes to low-level thermodynamic fields. Monthly Weather Review, 124(8), 1767-1785, 1996.

Cropp, Roger, Gabric, Albert, van Tran, Dien, Jones, Graham, Swan, Hilton, and Butler, Harry: Coral reef aerosol emissions in response to irradiance stress in the Great Barrier Reef, Australia. Ambio, 47(6), 671–681. https://doi.org/10.1007/s13280-018-1018-y, 2018.

Dagan, G., Koren, I., Altaratz, O., and Lehahn, Y.: Shallow convective cloud field lifetime as a key factor for evaluating aerosol effects. iScience, 10, 192–202. https://doi.org/10.1016/j.isci.2018.11.032, 2018.

Deschaseaux, E., E. Deschaseaux, G. Jones, and H. Swan: Dimethylated sulfur compounds in coral-reef ecosystems. Environmental Chemistry 13: 239–251. https://doi.org/10.1071/ en14258, 2016.

Eastman, R., Warren, S. G., and Hahn, C. J.: Variations in cloud cover and cloud types over the ocean from surface observations. 1954–2008, Journal of Climate, 24, 5914– 5934. https://doi.org/10.1175/2011JCLI3972.1, 2011.

Eastman, R., & Wood, R.: The Competing effects of stability and humidity on subtropical stratocumulus entrainment and cloud evolution from a Lagrangian perspective. Journal of the Atmospheric Sciences, 75(8), 2563–2578. https://doi.org/10.1175/JAS-D-18-0030.1. 2018.

Eleftheratos, K., Zerefos, C. S., Varotsos, C., and Kapsomenakis, I.: Interannual variability of cirrus clouds in the tropics in El Niño Southern Oscillation (ENSO) regions based on International Satellite Cloud Climatology Project (ISCCP) satellite data. International Journal of Remote Sensing, 32(21), 6395–6405. https://doi.org/10.1080/01431161.2010.510491, 2011.

Fiddes, S. L. Modelling the atmospheric influence of coral reef-derived dimethyl sulfide. 2020.

Fiddes, Sonya L, Woodhouse, Matthew T, Lane, Todd P, and Schofield, Robyn: Coral- reef-derived dimethyl sulfide and the climatic impact of the loss of coral reefs. Atmospheric Chemistry and Physics, 21(8), 5883–5903. https://doi.org/10.5194/acp-21-5883-2021, 2021.

Fiddes, S.L., Woodhouse, M.T., Utembe, S., Schofield, R., Alexander, S.P., Alroe, J., Chambers, S.D., Chen, Z., Cravigan, L., Dunne, E. and Humphries, R.S.: The contribution of coral-reef-derived dimethyl sulfide to aerosol burden over the Great Barrier Reef: a modelling study. Atmospheric Chemistry and Physics, 22(4), pp.2419-2445. 2022.

Filipiak, M. J., Merchant, C. J., Kettle, H., and Le Borgne, P.: An empirical model for the statistics of sea surface diurnal warming. Ocean Science, 8(2), 197-209, https://doi.org/10.5194/os-8-197-2012, 2012.

Fischer E, and Jones G.: Atmospheric dimethysulphide production from corals in the Great Barrier Reef and links to solar radiation, climate and coral bleaching. Biogeochemistry 110: 31–46, 2012.

Gentemann, C. L., C. J. Donlon, A. Stuart-Menteth, and F. J. Wentz: Diurnal signals in satellite sea surface temperature measurements, Geophys. Res. Lett., 30(3), 1140, doi:10.1029/2002GL016291, 2003.

Ghan, S. J., X. Liu, R. C. Easter, R. Zaveri, P. J. Rasch, J. Yoon, and B. Eaton: Toward a Minimal Representation of Aerosols in Climate Models: Comparative Decomposition of Aerosol Direct, Semidirect, and Indirect Radiative Forcing. J. Climate, 25, 6461–6476, https://doi.org/10.1175/JCLI-D-11-00650.1. 2012.

Gryspeerdt, E., Goren, T., Sourdeval, O., Quaas, J., Mülmenstädt, J., Dipu, S., Unglaub, C., Gettelman, A., and Christensen, M.: Constraining the aerosol influence on cloud liquid water path, Atmos. Chem. Phys., 19, 5331–5347, https://doi.org/10.5194/acp-19-5331-2019, 2019.

H. Wang, Easter, R. C., Rasch, P. J., M. Wang, X. Liu, Ghan, J., Y. Qian, J.-H. Yoon, Ma, P.-L., & Velu, V.: Sensitivity of remote aerosol distributions to representation of cloud-aerosol interactions in a global climate model. Geoscientific Model Development Discussions, 6(1), 331–378. https://doi.org/10.5194/gmdd-6-331-2013. 2013.

Han, Q., Rossow, W.B., Zeng, J. and Welch, R.: Three different behaviors of liquid water path of water clouds in aerosol–cloud interactions. Journal of the atmospheric sciences, 59(3), pp.726-735. 2002.

Herwitz, S.R.: Infiltration-excess caused by Stemflow in a cyclone-prone tropical rainforest. Earth Surface Processes and Landforms, 11(4), 401–412. https://doi.org/10.1002/esp. 3290110406, 1986.

Hersbach, H., de Rosnay, P., Bell, B., Schepers, D., Simmons, A., Soci, C., Abdalla, S., Alonso-Balmaseda, M., Balsamo, G., Bechtold, P. and Berrisfold, P.: Operational global reanalysis: Progress, future directions and synergies with NWP. ECMWF ERA Report Series, 27, 65, doi: 10.21957/tkic6g3wm, 2018.

Hersbach, H., Bell, B., Berrisford, P., Hirahara, S., Horányi, A., Muñoz-Sabater, J., Nicolas, J., Peubey, C., Radu, R., Schepers, D. and Simmons, A.: The ERA5 global reanalysis. Quarterly Journal of the Royal Meteorological Society, 146(730), 1999-2049, https://doi.org/10.1002/qj.3803, 2020.

Hughes, T.P., Kerry, J.T., Álvarez-Noriega, M., Álvarez-Romero, J.G., Anderson, K.D., Baird, A.H., Babcock, R.C., Beger, M., Bellwood, D.R., Berkelmans, R. and Bridge, T.C.: Global warming and recurrent mass bleaching of corals. Nature, 543(7645), 373–377. https://doi.org/10.1038/nature21707, 2017.

Hoffmann, F., and G. Feingold: Cloud Microphysical Implications for Marine Cloud Brightening: The Importance of the Seeded Particle Size Distribution. J. Atmos. Sci., 78, 3247–3262, https://doi.org/10.1175/JAS-D-21-0077.1. 2021.

Hong, Song-You, Yign Noh, and Jimy Dudhia: A new vertical diffusion package with an explicit treatment of entrainment processes. Monthly weather review 134.9, 2318- 2341, https://doi.org/10.1175/MWR3199.1, 2006.

Houze, R.A.: Orographic effects on precipitating clouds. Rev. Geophys. 50 RG1001, 47pp, https:// doi.org/10.1029/2011RG000365, 2012.

Imre, D., Abramson, E. and Daum, P.: Quantifying Cloud Induced Shortwave Absorption: An Examination of Uncertainties and of Recent Arguments for Large Excess Absorption. Journal of Applied Meteorology (1988–2005), 35(11), 1991–2010. https://doi.org/10.1175/1520-0450(1996)0352. 0.CO;2, 1996.

Jackson RL, Woodhouse MT, Gabric AJ, Cropp RA, Swan HB, Deschaseaux ESM and Trounce H.: Modelling the influence of coral-reef-derived dimethylsulfide on the atmosphere of the Great Barrier Reef, Australia. Mar. Sci.9:910423. doi: 10.3389/fmars.2022.910423. 2022.

Janjić, Zaviša I.: Comments on "Development and evaluation of a convection scheme for use in climate models". Journal of the Atmospheric Sciences 57.21:3686-3686, https://doi.org/10.1175/1520-0469(2000)057<3686:CODAEO>2.0.CO;2 , 2000.

Jo, H. S., Yeh, S. W., and Cai, W.: An episodic weakening in the boreal spring SST– precipitation relationship in the western tropical Pacific since the late 1990s. Journal of Climate, 32(13), 3837-3845, https://doi.org/10.1175/JCLI-D-17-0737.1, 2019.

Jones, G., Curran, M., Swan, H. and Deschaseaux, E.: Dimethylsulfide and Coral Bleaching: Links to Solar Radiation, Low Level Cloud and the Regulation of Seawater Temperatures and Climate in the Great Barrier Reef. American Journal of Climate Change, 6, 328-359. doi: 10.4236/ajcc.2017.62017, 2017.

Jones, G.B.: The reef sulphur cycle: Influence on climate and ecosystem services. In Ethnobiology of corals and coral reefs, ed. N.E. Narchi, and L.L. Price, 27–57. Cham: Springer, doi: 10.1007/978-3-319-23763-3_3, 2015.

Lawrence, M.G.: The relationship between relative humidity and the dewpoint temperature in moist air: a simple conversion and applications. Bulletin of the American Meteorological Soci- ety, 86, 225–233. https://doi.org/10.1175/BAMS-86-2-225. 2005.

Leahy, S. M., Kingsford, M. J., and Steinberg, C. R.: Do clouds save the Great Barrier Reef? Satellite imagery elucidates the cloud-SST relationship at the local scale. PLoS One, 8(7), e70400, https://doi.org/10.1371/journal.pone.0070400, 2013.

Lohmann, U, and Feichter, J.: Global indirect aerosol effects: A review. Atmospheric Chemistry and Physics, 5(3), 715–737. https://doi.org/10.5194/acp-5-715-2005, 2005.

Lu, R., and S. Lu: Local and remote factors affecting the SST– precipitation relationship over the western North Pacific during summer. J. Climate, 27, 5132–5147, https://doi.org/ 10.1175/JCLI-D-13-00510.1, 2014.

Milionis A. E. & Davies, T. D.: The effect of the prevailing weather on the statistics of atmospheric temperature inversions. International Journal of Climatology, 28(10), 1385–1397. https://doi.org/10.1002/joc.1613. 2008.

Mumby, P., Chisholm, J., Edwards, A., Andrefouet, S., and Jaubert, J.: Cloudy weather may have saved Society Island reef corals during the 1998 ENSO event, Marine Ecology Progress Series, 222, 209–216, https://doi.org/10.3354/meps222209, 2001.

Murphy, M J.: Variability in the trade wind regime and wet season of Northeastern Queensland, 2017.

Mlawer, E. J., Taubman, S. J., Brown, P. D., Iacono, M. J., and Clough, S. A.: Radiative transfer for inhomogeneous atmospheres: RRTM, a validated correlated-k model for the longwave. J. Geophys. Res. Atmos., 102, 16663, doi: 10.1029/97JD00237, 1997.

M. J. Weston, S. J. Piketh, F. Burnet, S. Broccardo, C. Denjean, T. Bourrianne, and P. Formenti: Sensitivity analysis of an aerosol-aware microphysics scheme in Weather Research and Forecasting (WRF) during case studies of fog in Namibia. Atmospheric Chemistry and Physics, 22, 10221–10245. https://doi.org/10.5194/acp-22-10221-2022, 2022.

Narenpitak, P., Bretherton, C. S., & Khairoutdinov, M. F.: Cloud and circulation feedbacks in a near-global aquaplanet cloud-resolving model. Journal of Advances in Modeling Earth Systems, 9, 1069–1090. https://doi.org/10.1002/2016MS000872. 2017.

Narenpitak, P. and Bretherton, C.S.: Understanding negative subtropical shallow cumulus cloud feedbacks in a near-global aquaplanet model using limited area cloud-resolving simulations. Journal of Advances in Modeling Earth Systems, 11(6), pp.1600-1626. 2019.

Norris, J. R.: Low cloud type over the ocean from surface observations. Part II: Geographical and seasonal variations. Journal of climate, 11(3), 383-403, https://doi.org/10.1175/1520-0442(1998)011<0383:LCTOTO>2.0.CO;2, 1998.

Nygård, T., Tjernström, M., and Naakka, T.: Winter thermodynamic vertical structure in the Arctic atmosphere linked to large-scale circulation, Weather Clim. Dynam., 2, 1263–1282, https://doi.org/10.5194/wcd-2-1263-2021, 2021.

Qu X, Hall A, Klein SA, and DeAngelis AM: Positive tropical marine low-cloud cover feedback inferred from cloud-controlling factors. Geophys Res Lett 42:7767–7775. Https://doi. org/10.1002/2015GL065627, 2015.

Rauber, R. M., Stevens, B., Ochs, H. T., Knight, C. A., Albrecht, B. A., Blyth, A. M., Fairall, C. W., and Jensen, J. B., Lasher-Trapp, S.G., Mayol-Bracero, O.L. and Vali, G.: Rain in shallow cumulus over the ocean: The RICO campaign. Bulletin of the American Meteorological Society, December 2007, 1912–1928. https://doi.org/10.1175/BAMS-88-12-1912, 2007.

Riehl, Herbert. Climate and Weather in the Tropics. Academic Press, 1979.

Rieck, M., Nuijens, L., & Stevens, B.: Marine boundary layer cloud feedbacks in a constant relative humidity atmosphere. Journal of the Atmospheric Sciences, 69(8), 2538–2550. https://doi.org/10.1175/JAS-D-11-0203.1. 2012.

Roe, G.H.: Orographic precipitation. Annu. Rev. Earth Planet. Sci. 33, 645–671. https://doi.org/10.1146/annurev.earth.33.092203.122541, 2005.

Sarmadi, F., Huang, Y., Thompson, G., Siems, S. T., and Manton, M. J.: Simulations of orographic precipitation in the Snowy Mountains of Southeastern Australia. Atmospheric Research, 219, 183-199, https://doi.org/10.1016/j.atmosres.2019.01.002, 2019.

Saffin, L., Blyth, A., Böing, S., Denby, L., Marsham, J., Lock, A., & Tomassini, L.: Kilometer-Scale Simulations of Trade-Wind Cumulus Capture Processes of Mesoscale Organization. Journal of Advances in Modeling Earth Systems, 15(3). https://doi.org/10.1029/2022MS003295. 2023.

Schneider, L., Barthlott, C., Barrett, A. I., and Hoose, C.: The precipitation response to variable terrain forcing over low mountain ranges in different weather regimes. Quarterly Journal of the Royal Meteorological Society, 144(713), 970-989, https://doi.org/10.1002/qj.3250, 2018.

Skamarock, W.C., Klemp, J.B., Dudhia, J., Gill, D.O., Liu, Z., Berner, J., Wang, W., Powers, J.G., Duda, M.G., Barker, D.M. and Huang, X.Y.: A description of the advanced research WRF version 4. NCAR tech. note ncar/tn-556+ str, 145, 2019.

Spill, G., Stier, P., Field, P. R., and Dagan, G.: Contrasting responses of idealised and realistic simulations of shallow cumuli to aerosol perturbations. Geophysical Research Letters, 48, e2021GL094137. https://doi.org/10.1029/2021GL094137, 2021.

Stevens B and Brenguier J-L: Cloud-controlling factors: low clouds Clouds in the Perturbed Climate System: Their Relationship to Energy Balance, Atmospheric Dynamics, and Precipitation ed J Heintzenberg and R J Charlson (Cambridge, MA: MIT Press) pp 173–196, https://doi.org/10.7551/mitpress/9780262012874.003.0008, 2009.

Stuart-Smith, R. D., Brown, C. J., Ceccarelli, D. M., and Edgar, G. J.: Ecosystem restructuring along the Great Barrier Reef following mass coral bleaching. Nature (London), 560(7716), 92–96. https://doi.org/10.1038/s41586-018-0359-9, 2018.

Sumner, G. and M. Bonell: Circulation and daily rainfall in the North Queensland wet seasons 1979–1982. Journal of Climatology, 6 (5), 531–549, https://doi.org/10.1002/joc.3370060507, 1986.

Smith, S.A., Vosper, S.B., and Field, P.R.: Sensitivity of orographic precipitation enhancement to horizontal resolution in the operational Met Office Weather forecasts. Meteorol. Appl. 22, 14–24. https://doi.org/10.1002/met.1352, 2015.

Takahashi, Naoya, Hayasaka, Tadahiro, Qiu, Bo, and Yamaguchi, Ryohei: Observed response of marine boundary layer cloud to the interannual variations of summertime Oyashio extension SST front. Climate Dynamics, 56(11-12), 3511–3526. https://doi.org/10.1007/s00382-021-05649-4, 2021.

Tao, W. K., Chen, J.-P., Li, Z., Wang, C., and Zhang, C.: Impact of Aerosols on boundary layer clouds and precipitation, Reviews of Geophysics, 50, 2011RG000 369, https://doi.org/10.1029/2011RG000369.1.INTRODUCTION, 2012.

Thompson, G., and Eidhammer, T.: A study of aerosol impacts on clouds and precipitation development in a large winter cyclone. Journal of the atmospheric sciences, 71(10), 3636-3658, https://doi.org/10.1175/JAS-D-13-0305.1, 2014.

Thompson, P. R. Field, R. M. Rasmussen, and W. D. Hall, 2008: Explicit forecasts of winter precipitation using an improved bulk mi- crophysics scheme. Part II: Implementation of a new snow parameterization. Mon. Wea. Rev., 136, 5095–5115, doi:10.1175/ 2008MWR2387.1.

Tian, Baijun, Waliser, Duane E, and Fetzer, Eric J.: Modulation of the diurnal cycle of tropical deep convective clouds by the MJO. Geophysical Research Letters, 33(20). https://doi.org/10.1029/2006GL027752, 2006.

Trier, S.B.: Convective storms – convective initiation. In: Holton, J.R., Curry, J.A. and Pyle, J.A. (Eds.) Encyclopedia of Atmospheric Sciences, Vol. 2. London: Academic Press, pp. 560–570, 2003.

Twomey, S.: The influence of pollution on the shortwave albedo of clouds. Journal of the Atmospheric Sciences, 34(7), 1149–1152. https://doi.org/10.1175/1520-0469(1977)034<1149:TIOPOT>2.0.CO;2, 1977.

Vogel, R., Nuijens, L., & Stevens, B.: The role of precipitation and spatial organization in the response of trade-wind clouds to warming. Journal of Advances in Modeling Earth Systems, 8, 843–862. https://doi.org/10.1002/2015MS000568. 2016.

Vogel, R., Nuijens, L., & Stevens, B.: Influence of deepening and mesoscale organization of shallow convection on stratiform cloudiness in the downstream trades. Quarterly Journal of the Royal Meteorological Society, 146(726), 174–185. https://doi.org/10.1002/qj.3664. 2020.

Warren, S G, Hahn, C J, London, J, Chervin, R M, and Jenne, R L.: Colorado Univ., Boulder, CO, Colorado Univ., Boulder, CO, and National Center for Atmospheric Research, Boulder, CO. Global distribution of total cloud cover and cloud type amounts over the ocean. United States: N. p., Web. doi:10.2172/5415329, 1988.

Weston, M., Piketh, S., Burnet, F., Broccardo, S., Formenti, P., and Laplace, S.: Sensitivity analysis of an aerosol aware microphysics scheme in WRF during case studies of fog in Namibia. Mesoscale model parameterisation of fog in arid environments, 129, https://doi.org/10.5194/acp-22-10221-2022, 2022.

Wheeler, M. C., and Hendon, H. H.: An all-season real-time multivariate MJO index: Development of an index for monitoring and prediction. Monthly weather review, 132(8), 1917-1932, https://doi.org/10.1175/1520-0493(2004)132<1917:AARMMI>2.0.CO;2, 2004.

Wilkinson, J. M., Porson, A. N. F., Bornemann, F. J., Weeks, M., Field, P. R., and Lock, A. P.: Improved microphysical parametrization of drizzle and fog for operational forecasting using the Met Office Unified Model, Q. J. Roy. Meteorol. Soc., 139, 488–500, https://doi.org/10.1002/qj.1975, 2013.

Wood, R., & Bretherton, C. S.: On the Relationship between Stratiform Low Cloud Cover and Lower-Tropospheric Stability. Journal of Climate, 19(24), 6425–6432. 2006.

Wu, B., T. Zhou, and T. Li: Contrast of rainfall–SST relationships in the western North Pacific between the ENSO-developing and ENSO-decaying summers. J. Climate, 22, 4398–4405, https://doi.org/10.1175/2009JCLI2648.1, 2009.

Wu, R., and B. P. Kirtman: Regimes of seasonal air–sea interaction and implications for performance of forced simulations. Climate Dyn., 29, 393–410, https://doi.org/10.1007/s00382-007-0246-9, 2007.

Wu, W., Liu, Y., and Betts, A. K.: Observationally based evaluation of NWP reanalyses in modeling cloud properties over the southern great plains. Journal of Geophysical Research. Atmospheres, 117(12) http://dx.doi.org/10.1029/2011JD016971, 2012.

Wyant, M. C., Bretherton, C. S., & Blossey, P. N.: Subtropical low cloud response to a warmer climate in a superparameterized climate model. Part I: Regime sorting and physical mechanisms. Journal of Advances in Modeling Earth Systems, 1, 7. https://doi.org/10.3894/JAMES.2009.1.7. 2009.

Yuan, Jian, and Houze JR, Robert A.: Deep convective systems observed by a-train in the tropical indo-pacific region affected by the MJO. Journal of the Atmospheric Sciences, 70(2), 465–486. https://doi.org/10.1175/JAS-D-12-057.1, 2013.

Zhang, S., Wang, M., Ghan, S.J., Ding, A., Wang, H., Zhang, K., Neubauer, D., Lohmann, U., Ferrachat, S., Takeamura, T. and Gettelman, A.: On the characteristics of aerosol indirect effect based on dynamic regimes in global climate models. Atmospheric Chemistry and Physics, 16(5), pp.2765-2783. 2016.

Zhang, H., H. Beggs, X. H. Wang, A. E. Kiss, and C. Griffin: Seasonal patterns of SST diurnal variation over the Tropical Warm Pool region, J. Geophys. Res. Oceans, 121, 8077–8094, doi:10.1002/ 2016JC012210, 2016.

Zhang, M., Rasmussen, K. L., Meng, Z., and Huang, Y.: Impacts of coastal terrain on warm-sector heavy-rain-producing MCSs in Southern China. Monthly Weather Review, 150(3), 603-624, https://doi.org/10.1175/MWR-D-21-0190.1, 2022.

Zhao, W., Huang, Y., Siems, S., and Manton, M.: The role of clouds in coral bleaching events over the Great Barrier Reef. Geophysical Research Letters, 48, e2021GL093936. https://doi. org/10.1029/2021GL093936, 2021.

Zhao, W., Y. Huang, Steven T. Siems, and Michael J. Manton: A characterization of clouds over the Great Barrier Reef and the role of local forcing, International Journal of Climatology, 1-18. https://doi.org/ 10.1002/joc.7660, 2022.